

## **Kinetics and products of chromium (VI) reduction by iron (II/III)-bearing clay minerals**

*Claresta Joe-Wong<sup>1\*</sup>†, Gordon E. Brown, Jr.<sup>1,2</sup>, Kate Maher*

<sup>1</sup>Department of Geological Sciences, School of Earth, Energy & Environmental Sciences,  
Stanford University, Stanford, CA 94305, USA (at time of publication)

<sup>2</sup>Department of Photon Science and Stanford Synchrotron Radiation Lightsource, SLAC National  
Accelerator Laboratory, 2575 Sand Hill Road, MS 69, Menlo Park, CA 94025, USA

\* Email address: [cjoewong@lbl.gov](mailto:cjoewong@lbl.gov)

† Present address: Earth and Environmental Sciences Area, Lawrence Berkeley National  
Laboratory, 1 Cyclotron Road, Berkeley, CA 94720, USA

This document is the unedited Author's version of a submitted work that was subsequently accepted for publication in *Environmental Science and Technology*, copyright © American Chemical Society after peer review. To access the final edited and published work (doi: 10.1021/acs.est.7b02934), see: <https://pubs.acs.org/doi/10.1021/acs.est.7b02934>.

# Kinetics and Products of Chromium(VI) Reduction by Iron(II/III)-Bearing Clay Minerals

*Claresta Joe-Wong<sup>1\*</sup>, Gordon E. Brown, Jr.<sup>1,2</sup>, Kate Maher<sup>1</sup>*

<sup>1</sup>Department of Geological Sciences, School of Earth, Energy & Environmental Sciences,  
Stanford University, Stanford, CA 94305, USA

<sup>2</sup>Department of Photon Science and Stanford Synchrotron Radiation Lightsource, SLAC National  
Accelerator Laboratory, 2575 Sand Hill Road, MS 69, Menlo Park, CA 94025, USA

\*Address: 450 Serra Mall, Bldg. 320, Rm. 118, Stanford, CA 94305, USA

Email address: joewongc@stanford.edu

## **Abstract**

Hexavalent chromium is a water-soluble pollutant whose mobility can be controlled by reduction of Cr(VI) to less soluble, environmentally benign Cr(III). Iron(II/III)-bearing clay minerals are widespread potential reductants of Cr(VI), but the kinetics and pathways of Cr(VI) reduction by such clay minerals are poorly understood. We reacted aqueous Cr(VI) with two abiotically reduced clay minerals: an Fe-poor montmorillonite and an Fe-rich nontronite. The effects of ionic strength, pH, total Fe content, and the fraction of reduced structural Fe(II) (Fe(II)/Fe(total)) were examined. The last variable had the largest effect on Cr(VI) reduction kinetics: for both clay minerals, the rate constant of Cr(VI) reduction varies by more than three orders of magnitude with

Fe(II)/Fe(total) and is described by a linear free energy relationship. Under all conditions examined, Cr and Fe K-edge X-ray absorption near-edge structure spectra show that the main Cr-bearing product is a Cr(III)-hydroxide and that Fe remains in the clay structure after reacting with Cr(VI). This study helps to quantify our understanding of the kinetics of Cr(VI) reduction by Fe(II/III)-bearing clay minerals and may improve predictions of Cr(VI) behavior in subsurface environments.

## Introduction

Chromium(VI) is an important groundwater pollutant that also occurs naturally in regions rich in ultramafic rocks.<sup>1,2</sup> Chromium(VI) is generally mobile in ground and surface waters,<sup>3</sup> whereas Cr(III) is an environmentally benign micronutrient<sup>4</sup> with low solubility.<sup>5</sup> Chromium oxidation and reduction have been extensively studied to better understand the behavior of Cr, especially in subsurface environments where Cr may be present in groundwater and drinking water supplies.<sup>6</sup> Although Cr(III) has few naturally occurring oxidants (*e.g.*, Mn(III,IV)-oxides),<sup>7,8</sup> many naturally occurring reductants can reduce Cr(VI) to Cr(III), including aqueous Fe(II)<sup>9-12</sup> and Fe(II)-bearing solids.<sup>13-22</sup> Knowledge of both the kinetics and thermodynamic favorability of each potential reductant is critical for assessing the fate of Cr(VI) in complex natural environments.

Iron(II/III)-bearing clay minerals are ubiquitous in subsurface systems and capable of reducing many contaminants, including organic pollutants,<sup>23,24</sup> radionuclides,<sup>25,26</sup> and Cr(VI).<sup>16-22</sup> Chromium(III) products of Cr(VI) reduction associate with the clay mineral particles, either residing in the interlayer space<sup>16,17</sup> or sorbing to edge sites.<sup>18,27,28</sup> By analogy with Cr(III) sorption on silica<sup>29</sup> and  $\gamma$ -Al<sub>2</sub>O<sub>3</sub>,<sup>30</sup> Cr(III) likely sorbs initially as mono-nuclear complexes before forming multi-nuclear complexes and ultimately three-dimensional precipitates as the sorption density of Cr(III) increases. A Cr(III)-bearing oxyhydroxide forms at high Cr loadings.<sup>22</sup> Although Cr(III) products

have been characterized, the kinetics of Cr(VI) reduction by Fe(II/III)-bearing clay minerals are poorly understood.

Factors that may affect reaction kinetics include ionic strength and pH, which may influence Cr(VI) sorption; the Fe content of the clay mineral, which may affect electron transfer pathways; and Fe(II)/Fe(total) ( $X_{Fe(II)}$ ) within the clay mineral. At circumneutral pH, Cr(VI) is primarily reduced by Fe(II) that resides within the clay mineral structure<sup>19</sup> or is sorbed on the clay mineral surface.<sup>31</sup> To facilitate electron transfer, Cr(VI) is expected to sorb to particle edges<sup>18,27,28</sup> or enter into the clay interlayer space,<sup>16</sup> although electron transfer through a mostly redox-inactive tetrahedral layer in the latter case may be difficult.<sup>32,33</sup> Theoretical calculations suggest that electron transfer through the tetrahedral layer should be extremely slow,<sup>34</sup> yet experimental evidence implies that electrons can transfer to Fe(II) sorbed on the basal surface.<sup>35</sup> Intra-layer electron hopping in Fe-rich clay minerals may enlarge the pool of available Fe(II) and enhance the reduction of edge-sorbed Cr(VI), but such hopping may be irrelevant if the clay mineral is Fe-poor or most Cr(VI) is sorbed to the basal surface.

$X_{Fe(II)}$  may affect the rate of Cr(VI) reduction because  $X_{Fe(II)}$  controls the effective standard reduction potential ( $E^{\circ}_{eff}$ ) of clay minerals.<sup>36-38</sup> Linear free energy relationships between log of the rate constant  $k$  and  $E^{\circ}_{eff}$  have been constructed for Cr(VI) reduction by aqueous Fe(II) complexes<sup>9</sup> and nitroaromatic reduction by Fe(II/III)-bearing clay minerals,<sup>23</sup> suggesting that such a relationship may describe Cr(VI) reduction by Fe(II/III)-bearing clay minerals. Previous studies of Cr(VI) reduction by Fe(II/III)-bearing clay minerals have only evaluated single values of  $X_{Fe(II)}$ ,<sup>16,22</sup> despite the potential for reaction kinetics to vary by orders of magnitude with systematic changes in  $X_{Fe(II)}$ . Such variation is especially important because imposing reducing conditions during reductive remediation of Cr(VI) may cause large changes in  $X_{Fe(II)}$ .<sup>39-41</sup>

In this study, we examined the kinetics of Cr(VI) reduction by two Fe(II/III)-bearing 2:1 clay minerals, an Fe-poor montmorillonite and an Fe-rich nontronite. The montmorillonite contains isolated Fe(O,OH)<sub>6</sub> octahedra, hindering intra-layer electron hopping.<sup>42</sup> In the nontronite, Fe(O,OH)<sub>6</sub> octahedra comprise the majority of the octahedral layer, permitting intra-layer electron hopping.<sup>32,43</sup> The effects of pH and ionic strength on Cr(VI) reduction were investigated to elucidate the reaction pathway, and each clay mineral was evaluated at several values of  $X_{Fe(II)}$ . Chromium- and Fe-bearing products were characterized with K-edge X-ray absorption near edge structure (XANES) spectroscopy.

## Materials and Methods

The montmorillonite (SWy-2, Ca<sub>0.52</sub>Na<sub>0.14</sub>K<sub>0.01</sub>(Al<sub>3.23</sub>Fe<sub>0.42</sub>Mg<sub>0.56</sub>)(Si<sub>7.89</sub>Al<sub>0.14</sub>)O<sub>20</sub>(OH)<sub>4</sub>)<sup>44</sup> and nontronite (NAu-2, M<sub>0.72</sub>(Al<sub>0.34</sub>Fe<sub>3.54</sub>Mg<sub>0.05</sub>)(Si<sub>7.55</sub>Al<sub>0.16</sub>Fe<sub>0.29</sub>)O<sub>20</sub>(OH)<sub>4</sub>)<sup>45</sup> used in this study were purchased from the Clay Minerals Society (<http://clays.org>). In their native state, almost all Fe within the clay mineral structure is Fe(III).<sup>16</sup> The clay minerals were sonicated and size fractionated (0.2-2 μm) to minimize impurities (<2 μm)<sup>46,47</sup> but allow easy separation of clay mineral and solution via syringe filtration (>0.2 μm). Size fractionation was verified with scanning electron microscopy and dynamic light scattering, and the only impurity detected by X-ray diffraction was a small amount of quartz associated with both clay minerals. The clay minerals were saturated with Na<sup>+</sup> through repeated suspension in 1 M NaCl and centrifugation to maintain consistency with their electrochemical characterization by Gorski *et al.* (2013).<sup>38</sup> X-ray fluorescence spectrometry indicates that the montmorillonite contains 2.3 wt. % Fe and the nontronite 23.7 wt. % Fe, consistent with literature values.<sup>16,19,44,47,48</sup>

Further manipulations of the two clay minerals were performed in an anaerobic glovebox. Acid-washed glassware and plasticware were allowed to equilibrate with the glovebox atmosphere for at least 24 hours. Aqueous solutions were made with doubly deionized (DDI) water that had been sparged with  $N_2$  and allowed to equilibrate for at least 24 hours in the glovebox. Centrifugation was performed outside the glovebox in capped tubes held in aerosol-tight rotor buckets.

Clay minerals were reduced by sodium dithionite following a standard procedure.<sup>49,54</sup> In brief, each clay mineral was suspended in a sodium citrate/bicarbonate buffer to minimize clay dissolution. After adding sodium dithionite, the clay mineral was repeatedly washed with DDI water and size fractionated. The extent of reaction was controlled by varying the duration and temperature of reaction or by using only the stoichiometric amount of sodium dithionite.  $X_{Fe(II)}$  was determined by linear least-squares fitting of Fe K-edge XANES spectra with the spectra of the fully oxidized and fully reduced clay minerals serving as model compounds (**Figure S1**).  $E_{eff}^{\circ}$  was calculated with a modified Nernst equation using the parameters in Gorski *et al.* (2013) for pH 7.5.<sup>38</sup> The effects of pH on  $E_{eff}^{\circ}$  for the montmorillonite have not been experimentally determined but are likely minimal because Fe reduction and oxidation are not accompanied by proton transfer.<sup>55</sup> The effects of pH on  $E_{eff}^{\circ}$  on the nontronite are discussed below.

Chromium(VI) reduction experiments were carried out in constantly stirred batch reactors buffered at pH 7.3 or 5.5 by 0.5 mM sodium 4-(2-hydroxyethyl)-1-piperazineethanesulfonate (HEPES) or sodium acetate, respectively. These pH values were chosen to evaluate the importance of edge-site Cr(VI) or Cr(III) sorption while minimizing clay mineral dissolution, which increases at pH <4 or >8.<sup>19</sup> At pH 7.3, the edge sites of both clay minerals are negatively charged,<sup>56,57</sup> and 96% of Cr(VI) is present as  $CrO_4^{2-}$ . At pH 5.5, the edge sites of both clay minerals are positively charged,<sup>56,57</sup> and 72% of Cr(VI) is present as  $HCrO_4^-$ . Ionic strength was varied using several salts,

including sodium sulfate and calcium chloride. The montmorillonite was tested at five values of  $X_{\text{Fe(II)}}$  (0.34-0.95) and the nontronite at four different values of  $X_{\text{Fe(II)}}$  (0.26-0.98). Separate control experiments were performed to evaluate Cr(VI) stability in the presence of each buffer and each native, fully oxidized clay mineral (see **SI**). Every experiment was replicated at least once.

To keep  $X_{\text{Fe(II)}}$  and  $E^{\circ}_{\text{eff}}$  of the clay reasonably constant over the course of the experiment, the starting molar Cr(aq):Fe(clay mineral) ratio was 0.033 for the montmorillonite reactors and 0.017 for the nontronite reactors. Total Fe was kept constant instead of Fe(II) so that clay minerals with different  $X_{\text{Fe(II)}}$  values would have similar surface areas. Suspension densities were 0.73 g/L for the montmorillonite and 0.14 g/L for the nontronite, corresponding to  $[\text{Fe}]_0 = 300 \mu\text{M}$  and  $600 \mu\text{M}$  respectively. The clay mineral, buffer, and any salts were allowed to equilibrate overnight before initiating the reaction by adding  $10 \mu\text{M}$  Cr(VI). Aliquots were taken periodically and immediately passed through a  $0.2 \mu\text{m}$  polyethersulfone (PES) syringe filter to arrest the reaction. Chromium(VI) concentrations in the filtered aliquots were determined spectrophotometrically using diphenylcarbazide,<sup>58</sup> and Fe(II) and Fe(III) concentrations were determined spectrophotometrically using ferrozine.<sup>59</sup> Absorbances of gravimetric standards were reproducible within 3%.

Solid reactants and products were characterized using Cr and Fe K-edge XANES spectroscopy, which was carried out at beamlines 4-1 and 11-2 at the Stanford Synchrotron Radiation Lightsource as described in the **SI**. The initial concentration of Cr(VI) was varied to produce molar Cr(aq):Fe(clay mineral) ratios from 0.00033 to 0.33. XANES scans were calibrated and averaged in SixPack<sup>60</sup> before being normalized using Demeter software<sup>61</sup> by fitting a first-order polynomial to the pre-edge region and a second-order polynomial to the post-edge region. Chromium and Fe

speciation were determined by linear least squares fitting to a library of XANES spectra of Cr- and Fe-bearing standards.<sup>62</sup>

Scanning transmission X-ray microscopy (STXM) was performed on nontronite reaction products at beamline 5.3.2.2 at the Advanced Light Source and the Soft X-ray Spectromicroscopy beamline at the Canadian Light Source, as detailed in the **SI**. The lower Fe and Cr concentrations of the montmorillonite reaction products did not allow them to be imaged with STXM, nor did scanning electron microscopy allow the distribution or morphology of Cr products to be characterized in detail due to the low electrical conductivity of both clay minerals.

## Results and Discussion

### *Chromium(VI) Reduction Kinetics and Pathway*

Aqueous Cr(VI) concentrations decreased in every reactor containing reduced clay minerals. Aqueous Fe(II) concentrations were below the ferrozine detection limit (~0.1  $\mu\text{M}$ ), and control reactors containing Cr(VI), buffer, and unreduced clay minerals showed no significant decreases in aqueous Cr(VI) concentrations from reduction by the buffer or sorption by the clay minerals (**Figure S2**). The kinetics are consistent with a second-order rate law (**eq 1, Figure 1**):

$$\frac{d[\text{Cr(VI)}]}{dt} = -k[\text{Cr(VI)}] \left( \frac{X_{\text{Fe(II)}} \times f_{\text{Fe}} \times d_{\text{clay}}}{MW_{\text{Fe}}} \right) \quad (1)$$

where  $k$  is the second-order rate constant ( $\text{M}^{-1}\text{min}^{-1}$ ). The last term represents the concentration of Fe(II) and is calculated from  $X_{\text{Fe(II)}}$ ;  $f_{\text{Fe}}$ , the weight fraction of Fe in the clay mineral (g Fe/g clay mineral);  $d_{\text{clay}}$ , the clay mineral suspension density (g clay mineral/L); and  $MW_{\text{Fe}}$ , the molecular weight of Fe (g/mol). Changes in  $X_{\text{Fe(II)}}$  over the course of the reaction were calculated by assuming a stoichiometric 3:1 reaction with the lost Cr(VI).

Due to the excess of Fe(II) necessary to minimize changes in  $X_{Fe(II)}$ , the kinetics approach a pseudo-first-order model with respect to Cr(VI) (**Figure S3**). However, pseudo-first-order rate constants  $k_i$  ( $\text{min}^{-1}$ ) cannot be used to compare clay minerals with different values of  $X_{Fe(II)}$  because the concentration of Fe(II), which is embedded in  $k_i$ , depends on  $X_{Fe(II)}$  (**eq 1**). When  $Q_{clay}$  is halved,  $k_i$  also decreases by roughly half, which suggests that the reaction is first order with respect to Fe(II) and second order overall (**Figure S4**). Thus, to allow comparison amongst different  $X_{Fe(II)}$  values, second-order rate constants are used in the remainder of the text.

Second-order kinetics are consistent with previous studies of Fe(II/III)-bearing clay minerals. A second-order rate law was observed for Cr(VI) reduction by biotically reduced clay minerals<sup>16</sup> and nitroaromatic reduction by a low-Fe, abiotically reduced montmorillonite.<sup>63</sup> Nitroaromatic and organochlorine reduction by a Fe-rich, abiotically reduced smectite followed a more complex, biphasic second-order kinetic model involving two interconvertible Fe(II) species of differing reactivity.<sup>63,64</sup> Although the abiotically reduced nontronite may contain multiple types of Fe(II) sites with different reactivities towards Cr(VI),<sup>38,45</sup> multi-phase kinetics were not observed in our experiments:  $R^2$  values for a single-species, second-order model are greater than 0.9 under all conditions (**Tables S1 and S2**).

For highly reduced clay minerals, more Cr(VI) is lost in the initial seconds before the first sampling point than predicted by the second-order kinetics that describe the rest of the reaction. Although previously attributed to sorption,<sup>22</sup> this lost Cr(VI) is more likely reduced by residual Fe(II)-containing complexes sorbed on the clay surface, which is one of the fastest reductants of Cr(VI).<sup>31</sup> Surface-complexed Fe(II) may derive from the reduction of the clay minerals by sodium dithionite, which causes minor release of Fe(II) from the clay mineral structure.<sup>57</sup> Because sorbed Fe(II) reacts with Cr(VI) much faster than Fe(II) in the clay mineral structure, it is swiftly depleted

and does not appear to compete with structural Fe(II) over the course of the reaction beyond the initial sampling point. The dominant reductant beyond the first sampling point in all reactors is therefore assumed to be structural Fe(II). All structural Fe in the montmorillonite is octahedral.<sup>42</sup> As much as 8% of Fe in the nontronite structure is tetrahedral.<sup>45</sup> This tetrahedral Fe may be redox-active<sup>33</sup> but is likely not the major reductant of Cr(VI) for the nontronite, as discussed below.

Under our experimental conditions, reduction of all Cr(VI) by Fe(II) at edge sites is impossible without intra-layer electron hopping. If all Cr(VI) is edge-sorbed and no intra-layer electron hopping occurs, a concentric reaction front moving towards the interior of the clay mineral particle should develop. Dynamic light scattering indicates that clay mineral particles are somewhat larger than their nominal maximum of 2  $\mu\text{m}$  under experimental conditions, likely due to aggregation. A conservative back-of-the-envelope calculation assuming reaction of 5% of a flat circular particle 2  $\mu\text{m}$  in diameter implies that the distance of electron transfer would increase by the end of the reaction to more than 250  $\text{\AA}$ , compared to typical outer-sphere electron transfer distances of less than 15  $\text{\AA}$  in aqueous solutions.<sup>65</sup> Electron hopping over such large distances between the isolated Fe sites in the montmorillonite is expected to be extremely slow. However, extensive electron transfer remains possible for the nontronite because electron hopping between adjacent Fe(II/III) sites in the octahedral layer<sup>33,51</sup> is fast ( $\sim 10^6$  transfers/s).<sup>32</sup> Under these conditions, Cr(VI) therefore must primarily sorb on the montmorillonite basal plane to be reduced, but Cr(VI) sorbed on the nontronite edges or basal planes may be reduced.

To further constrain the reaction pathway, ionic strength and pH were varied. For the montmorillonite, inner-sphere Cr(VI) sorption on the basal plane is unlikely due to the negative charge on  $\text{CrO}_4^{2-}$  or  $\text{HCrO}_4^-$  and high oxidation state of Cr(VI). An O(-II) bridge between tetrahedral Cr(VI) and tetrahedral Si(IV) or Al(III) would carry an excess of positive charge in violation of

Pauling's second rule, although an inner-sphere bond between Cr(VI) and tetrahedral Fe(II) is theoretically possible.<sup>66</sup> Consistent with outer-sphere sorption of Cr(VI), increasing the ionic strength slows the reaction (**Figure 2A**). No significant differences were seen amongst the background electrolytes, which included  $\text{SO}_4^{2-}$  and  $\text{Cl}^-$  anions and  $\text{Na}^+$  and  $\text{Ca}^{2+}$  cations. The indifference to the anion identity suggests that the decrease in  $k$  is not due to competition for inner-sphere sorption sites, which are in any case unlikely to be favorable for sorption.<sup>67</sup> The indifference to the cation identity ( $\text{Na}^+$  vs.  $\text{Ca}^{2+}$ ) suggests that the decrease in  $k$  is not caused by collapse of the electrical double layer, aggregation of the clay mineral particles, or decreased clay mineral dissolution and release of aqueous  $\text{Fe}^{2+}$ .  $\text{Ca}^{2+}$  causes greater changes to the double layer, more clay mineral aggregation, and less dissolution than  $\text{Na}^+$ .<sup>67</sup> Furthermore, if the reaction is controlled by surface area, then lowering the pH, which is also expected to increase aggregation and decrease dissolution, should in turn decrease the reaction rate.

Instead, pH has no consistent effect on  $k$ , even though  $\text{HCrO}_4^-$  has a higher  $E^\circ$  (1.2 V) than  $\text{CrO}_4^{2-}$  (-0.12 V) and the edge charge changes from negative at pH 7.3 to positive at pH 5.5 (**Figure 2B**).<sup>56,68</sup> The lack of a pH effect is consistent with outer-sphere basal plane sorption, in contrast with previous studies that found exclusive Cr(VI) sorption to biotite and phlogopite edge sites.<sup>27,28,18</sup> Despite the electrostatic unfavorability of anionic Cr(VI) sorption to the negatively charged basal plane, it remains possible if the chemical potential of sorption is great.<sup>69</sup> Slight outer-sphere sorption of anionic Cr(VI) to negatively charged surfaces has been observed,<sup>70,71</sup> and even minor formation of an outer-sphere sorption complex as an unstable intermediate would allow the reaction to proceed. The precise mechanism for reduction of sorbed Cr(VI) cannot be determined due to the difficulty of observing Cr(V) or Cr(IV) intermediates. Thus, it remains unclear whether basal-plane-sorbed Cr(VI) is reduced by three separate Fe(II) sites or by a single Fe(II) site that is

regenerated by intra-layer electron hopping. Alternatively, Cr(V) and Cr(IV) intermediates may persist long enough on the clay surface for Cr disproportionation. As discussed in the next section, the collective results imply that the rate-determining step follows the first electron transfer.

For the nontronite, increasing the ionic strength slows the reaction to an even greater extent and does not depend on the identity of the background electrolyte (**Figure 3A**). Similarly to the montmorillonite, the decrease of  $k$  is thus consistent with outer-sphere sorption.<sup>67</sup> Cr(VI) reduction is faster at pH 5.5 than at pH 7.3 at every  $X_{\text{Fe(II)}}$  tested (**Figure 3B**). Reduction may be faster at the lower pH because  $\text{HCrO}_4^-$  has a higher  $E^\circ$  than  $\text{CrO}_4^{2-}$ ,<sup>68</sup> but this does not affect  $k$  for the montmorillonite, and  $E^\circ_{\text{eff}}$  of the nontronite is also expected to increase with decreasing pH.<sup>72</sup> A more likely explanation is that a significant fraction of the anionic Cr(VI) sorbs as an outer-sphere complex on the clay mineral edge, which is negatively charged at pH 7.3 but positively charged at pH 5.5.<sup>57</sup> Sorption of anionic Cr(VI) is hence more electrostatically favorable at the lower pH. Cr(VI) sorption on the basal plane followed by reduction by either octahedral or tetrahedral Fe(II) cannot be ruled out but is unlikely to lead to the observed pH dependence, since the diffuse negative charge on the basal plane does not depend on pH. Tetrahedral Fe is far less abundant than octahedral Fe and so is unlikely to be the major reductant of outer-sphere edge-sorbed Cr(VI).

### *Linear Free Energy Relationships*

The dominant influence on reaction kinetics for both clay minerals is the average  $X_{\text{Fe(II)}}$  as expressed by  $E^\circ_{\text{eff}}$ . Ionic strength and pH change  $k$  by less than an order of magnitude, whereas altering  $X_{\text{Fe(II)}}$  causes  $k$  to vary by three orders of magnitude (**Tables S1 and S2**). The dependence of  $k$  on  $E^\circ_{\text{eff}}$  can be described with a linear free energy relationship between  $\log(k)$  and  $E^\circ_{\text{eff}}$  for both clay minerals at pH 7.3 and 5.5, although the correlation is somewhat stronger for the

montmorillonite (**Figure 4**). As originally derived from Marcus theory for homogeneous electron transfer,<sup>65,73,74</sup> the slope of the linear free energy relationship can be used to assess the rate-determining step even in heterogeneous systems.<sup>23,63,75</sup> For a generic room temperature transfer of  $n$  electrons with the rate constant  $k_{ET}$ , the slope  $m_{ET}$  of the linear correlation between  $\log(k_{ET})$  and  $E_{eff}^{\circ}$  can be written as<sup>65</sup>

$$m_{ET} = -\frac{nF}{2.303RT} = -16.9n \text{ V}^{-1} \quad (2)$$

For both clay minerals, the observed slope is smaller than the ideal value for a single electron transfer of  $-16.9 \text{ V}^{-1}$ :  $-9.4 \pm 0.7 \text{ V}^{-1}$  at pH 7.3 and  $-7.5 \pm 1 \text{ V}^{-1}$  at pH 5.5 for the montmorillonite and  $-3.5 \pm 0.6 \text{ V}^{-1}$  at pH 7.3 and  $-3.0 \pm 0.8 \text{ V}^{-1}$  at pH 5.5 for the nontronite. These differences likely indicate that the observed rate constant  $k$  incorporates rate constants for other steps that do not involve electron transfer, decreasing the dependence of  $k$  on  $E_{eff}^{\circ}$ .<sup>76</sup> Examples of such steps may include Cr(VI) sorption prior to electron transfer, changes in the coordination geometry of Cr(V) or Cr(IV) after electron transfer, or structural alterations of edge-site Fe(II/III) that do not involve electron transfer.<sup>55,77</sup> Although the precise mechanism is unclear, the linear free energy relationship allows the kinetics of Cr(VI) reduction to be modeled over a spectrum of  $E_{eff}^{\circ}$  values.

### *Products*

Solid products were investigated using Cr and Fe K-edge XANES spectroscopy for both clay minerals under all pH and ionic strength conditions and a variety of buffer concentrations and Cr(aq):Fe(clay mineral) ratios. All Cr K-edge XANES spectra we measured are consistent with that of a Cr(III)-hydroxide, possibly admixed with Fe(III) (**Figures 5, S5, S6**). The absent pre-edge feature at 5993 eV and the strong absorption maximum at 6009 eV show that no significant

Cr(VI) is present in the solids and thus that sorbed Cr(VI) is reduced to Cr(III). Neither  $X_{\text{Fe(III)}}$  nor pH affects the products (**Figures 5 and S5**). Lowering the initial Cr(aq):Fe(clay mineral) ratio accentuates the dip in the main edge at 6014.5 eV, which may qualitatively indicate that the Cr(III)-hydroxide is enriched in Fe(III) (**Figure S6**).<sup>22</sup> Potential sources of Fe(III) in the Cr(III)-hydroxide include surface-sorbed Fe(II) and minor clay mineral dissolution during reaction.

Iron K-edge XANES spectra demonstrate that Fe(III) largely remains within the clay mineral structure after reaction (**Figure 6**). Spectra of the reduced clay minerals after reaction with Cr(VI) can be fit with linear combinations of the spectra for the unaltered, fully oxidized clay mineral and the reduced clay mineral prior to reaction with Cr(VI). The fraction of Fe in the products that is re-oxidized is roughly stoichiometrically equivalent to the amount of Cr(VI) lost from solution (**Table S3**). Redox cycling of Fe-rich clay minerals causes internal rearrangements of Fe among octahedral sites and (de)protonation reactions.<sup>51,77</sup> In addition, high levels of abiotic reduction can release as much as 35% of total Fe from the clay mineral structure.<sup>78</sup> To assess whether re-oxidation by Cr(VI) similarly releases Fe, the fully reduced nontronite was reacted for two weeks with stoichiometric Cr(VI) at pH 7.3 and 5.5. No Fe(II) or Fe(III) was detected in solution, and despite the near total oxidation of Fe(II) in the clay minerals, neither Fe(III)-oxyhydroxides nor any other Fe-bearing phases were detected. Iron K-edge XANES spectra of these reacted solids can be fit with linear combinations of the spectra for the oxidized and reduced nontronite endmembers, which imply that 100% of Fe(II) the nontronite was oxidized at pH 7.3 and 73% at pH 5.5 (**Figure S7**). The high surface area of clay minerals likely makes Fe-bearing clay minerals less susceptible to surface passivation by the Cr(III)-hydroxide product than other solid reductants such as magnetite.<sup>13,15</sup>

### *Implications for Modeling of Reaction Kinetics*

The rate of Cr(VI) reduction by Fe(II/III)-bearing clay minerals is primarily controlled by  $X_{Fe(II)}$ , which may simplify geochemical modeling of clay mineral-Cr(VI) systems. The Fe content of the clay mineral, pH, and ionic strength have only minor effects on the rate constant  $k$ , even though the high Fe content of the nontronite allows Cr(VI) reduction to follow a different reaction pathway. Cr(VI) reduction by the montmorillonite likely proceeds at basal surface sites as outer-sphere complexes, whereas Cr(VI) reduction by the nontronite likely proceeds at edge sites as outer-sphere complexes (**Figure 7**). Nevertheless, despite the different reaction mechanisms, rate-determining steps, and relationships between  $X_{Fe(II)}$  and  $E^{\circ}$ , the relationship between  $X_{Fe(II)}$  and  $k$  is almost identical for both clay minerals (**Figure S8**).

To illustrate the effects of  $X_{Fe(II)}$ , the kinetics of Cr(VI) reduction were modeled for a well-mixed system at pH 5.5 that contains two reductants, aqueous Fe(II) and the reduced montmorillonite (**Figure 8**). Sorption and possible redox reactions between the two reductants were not included. The ratio  $r$  of clay mineral Fe(II):aqueous Fe(II) was varied by several orders of magnitude, and  $X_{Fe(II)}$  was varied from 0.95 to 0.10. Aqueous Fe(II) is a faster reductant than the montmorillonite at all values of  $X_{Fe(II)}$ .<sup>12</sup> When  $r < 1$ , the effective rate constant for the system as a whole,  $k_{eff}$ , approaches the rate constant for aqueous Fe(II), and  $X_{Fe(II)}$  has little effect on  $k_{eff}$ . However, as  $r$  increases and the montmorillonite becomes the dominant reductant,  $X_{Fe(II)}$  becomes significant:  $k_{eff}$  varies by more than an order of magnitude with  $X_{Fe(II)}$  when  $r = 100$  and more than three orders of magnitude when  $r > 10^4$ . Linear free energy relationships, which allow rate constants to be estimated over orders of magnitude from limited experimental data, are thus invaluable for modeling Cr(VI) redox kinetics.

More work is needed to assess the reactivity of Fe(II/III)-bearing clay minerals in natural systems. The fast kinetics at high  $X_{Fe(II)}$ , lack of surface passivation effects, and ubiquity of Fe(II/III)-

bearing clay minerals may make them the dominant reductant in environments where little aqueous or sorbed Fe(II) is available for electron transfer reactions. Even when Fe(II/III)-bearing clay minerals are kinetically outcompeted as direct reductants of Cr(VI), they remain indirect, renewable sources of electrons.<sup>51,79</sup> In oxic settings where  $X_{Fe(II)}$  is very small, the kinetics of Cr(VI) reduction by these clay minerals may be similar ( $k \ll 0.05 \mu\text{M}^{-1}\text{yr}^{-1}$ ) to typical rates of Cr(VI) production from Cr(III) oxidation by Mn(III,IV) oxides in serpentinite soils ( $0.02\text{-}3 \mu\text{mol Cr(VI)/kg soil/yr}$ ).<sup>3</sup> The strong dependence of the kinetics of Cr(VI) reduction by Fe(II/III)-bearing clay minerals on  $X_{Fe(II)}$  and ultimately on the ambient redox conditions demonstrates the importance of evaluating the kinetics of heterogeneous Cr(VI) reduction as a function of thermodynamic favorability.

Table of Contents/Abstract Art

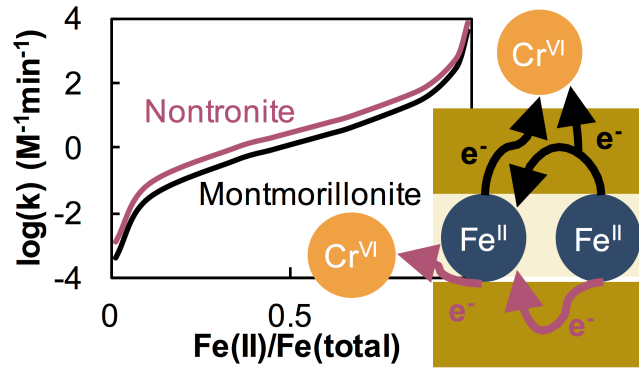


**Figure 1.** Second-order rate constants were determined by linear least-squares fitting for Cr(VI) reduction by (A) montmorillonite and (B) nontronite.  $X_{Fe(II)} = 0.49$  for the montmorillonite and 0.98 for the nontronite. Both reactors were buffered at pH 7.3, and  $[Cr(VI)]_0 = 10 \mu M$ . Error bars are smaller than the symbols.

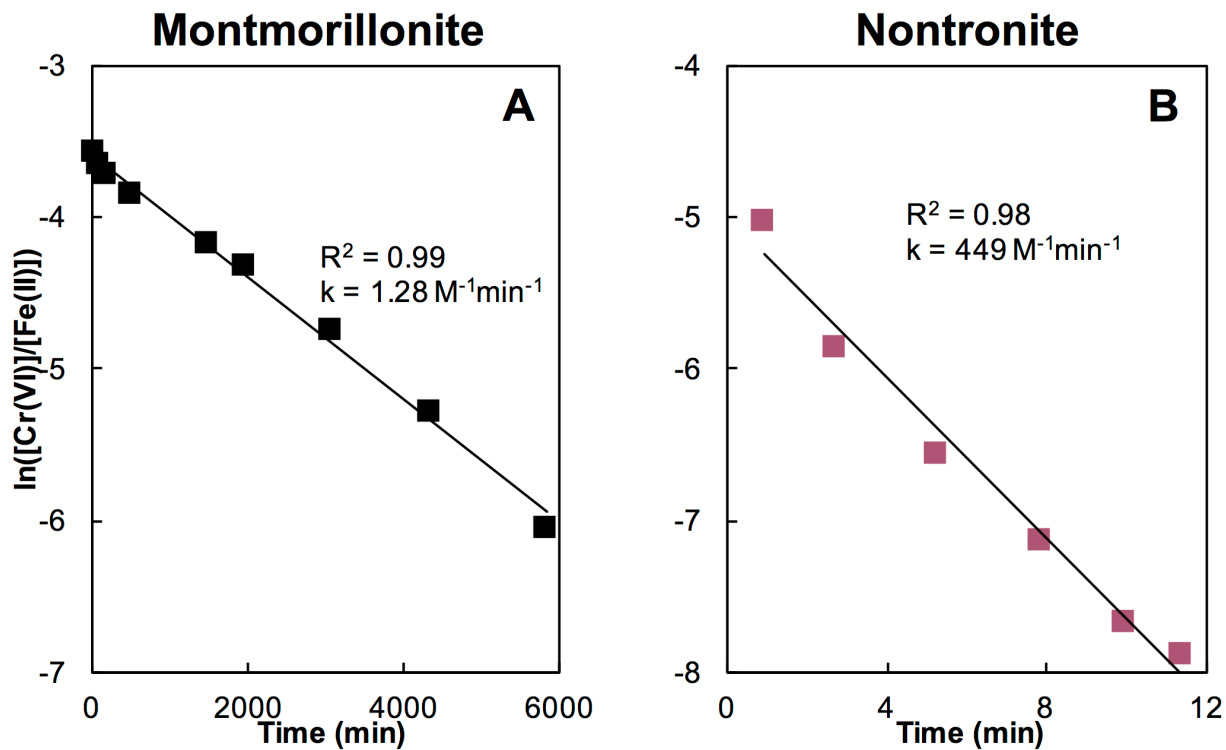


**Figure 2.** Effects of (A) ionic strength and (B) pH on Cr(VI) reduction by montmorillonite. Error bars in A show 3% variability in [Cr(VI)] and are in some cases smaller than the symbols; error bars in B show standard deviations from replicate experiments. All reactors were buffered with 0.5 mM sodium HEPES or acetate.

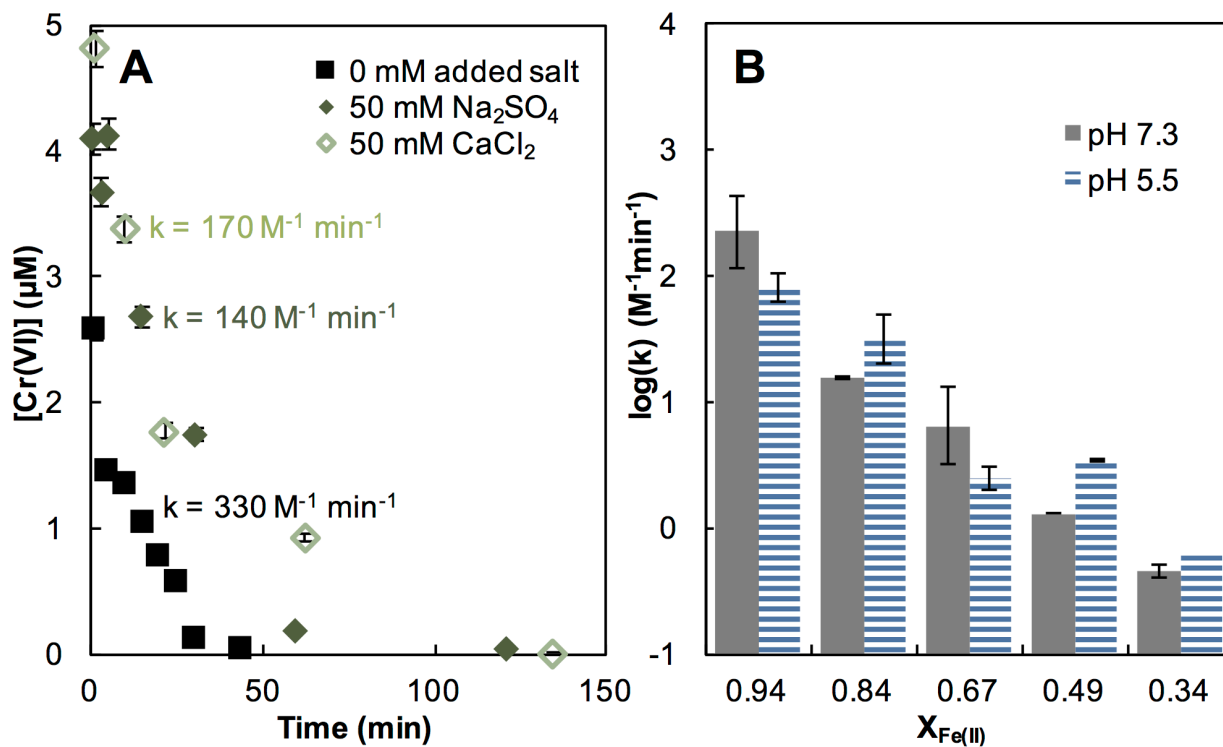


**Figure 3.** Effects of (A) ionic strength and (B) pH on Cr(VI) reduction by nontronite. Error bars in A show 3% variability in [Cr(VI)] and are in some cases smaller than the symbols; error bars in B show standard deviations from replicate experiments. All reactors were buffered with 0.5 mM sodium HEPES or acetate.

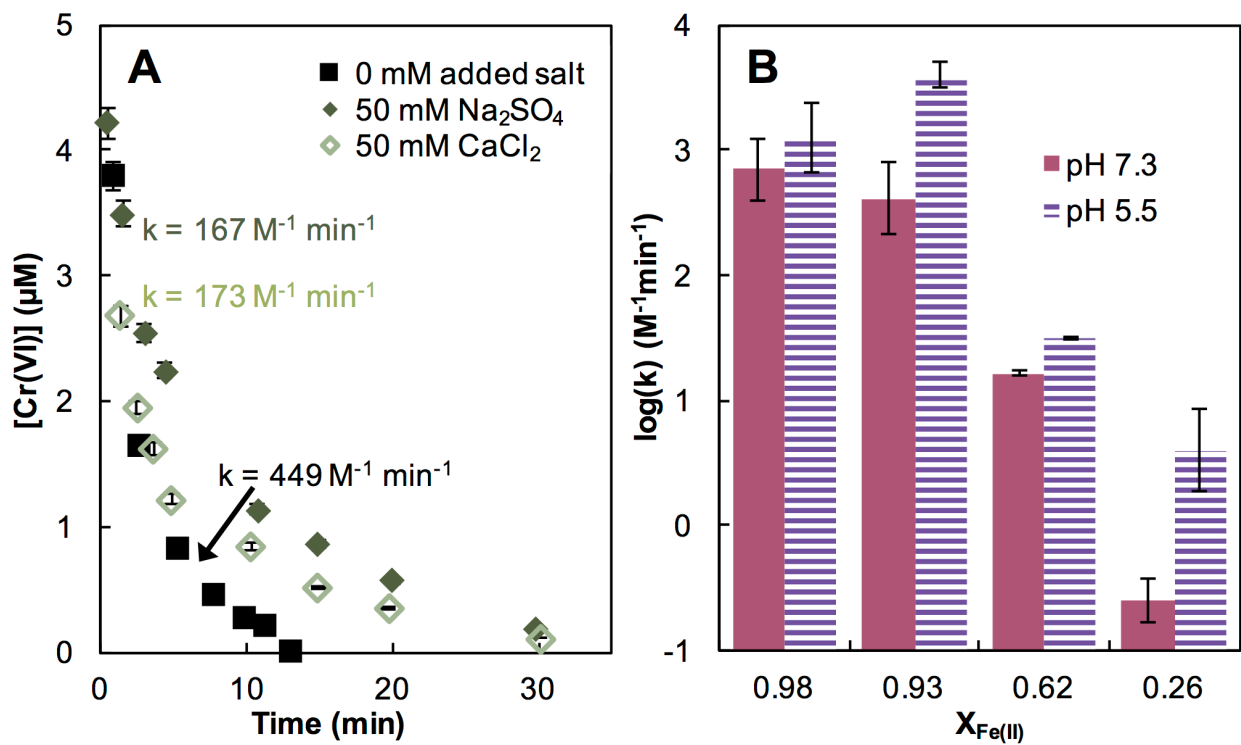


**Figure 4.** Second-order rate constants of Cr(VI) reduction as a function of  $E^{\circ}_{eff}$  for (A) montmorillonite and (B) nontronite. Rate constants at pH 7.3 are shown as filled squares; rate constants at pH 5.5 are shown as open circles. Lines show linear least-squares fit. Vertical error bars show standard deviations for replicate experiments. Horizontal error bars are derived from 5% error in linear combination fitting for  $X_{Fe(III)}$ .

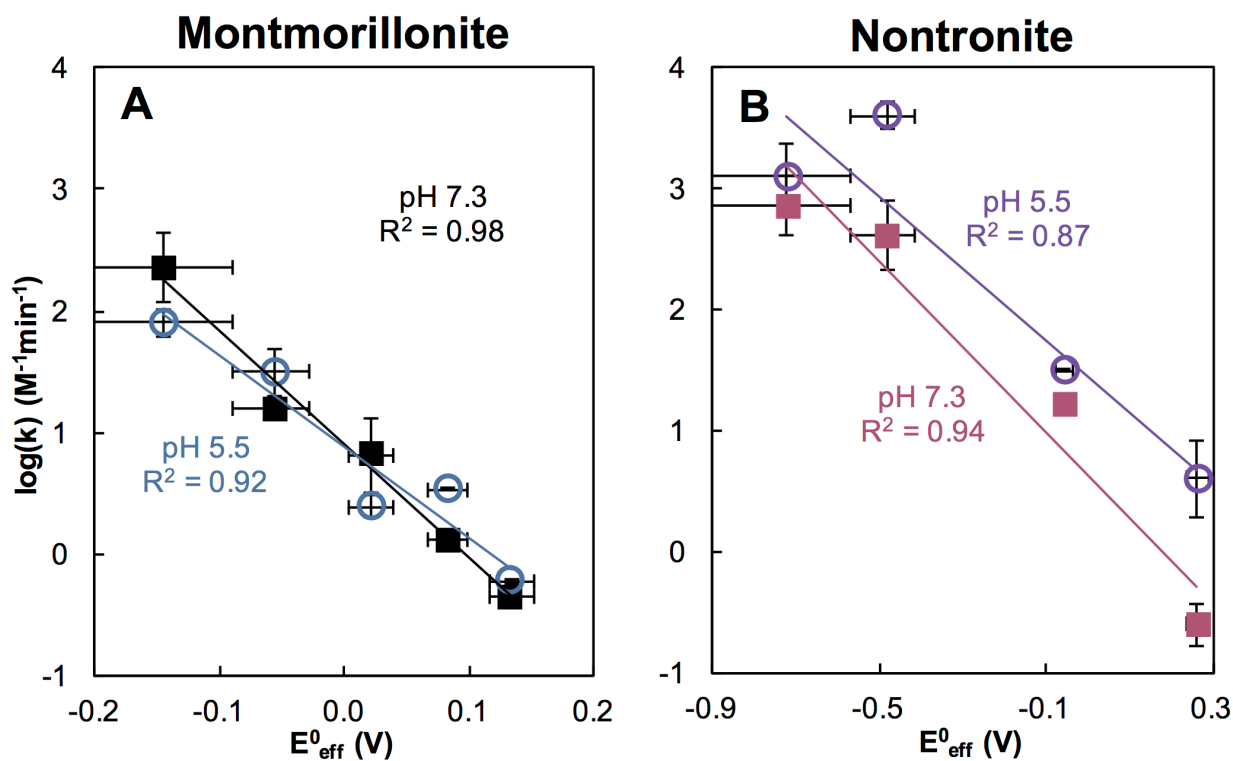


**Figure 5.** Cr K-edge XANES spectra of reacted solids (top three spectra) and standards (bottom three spectra). All reactors were buffered at pH 7.3.

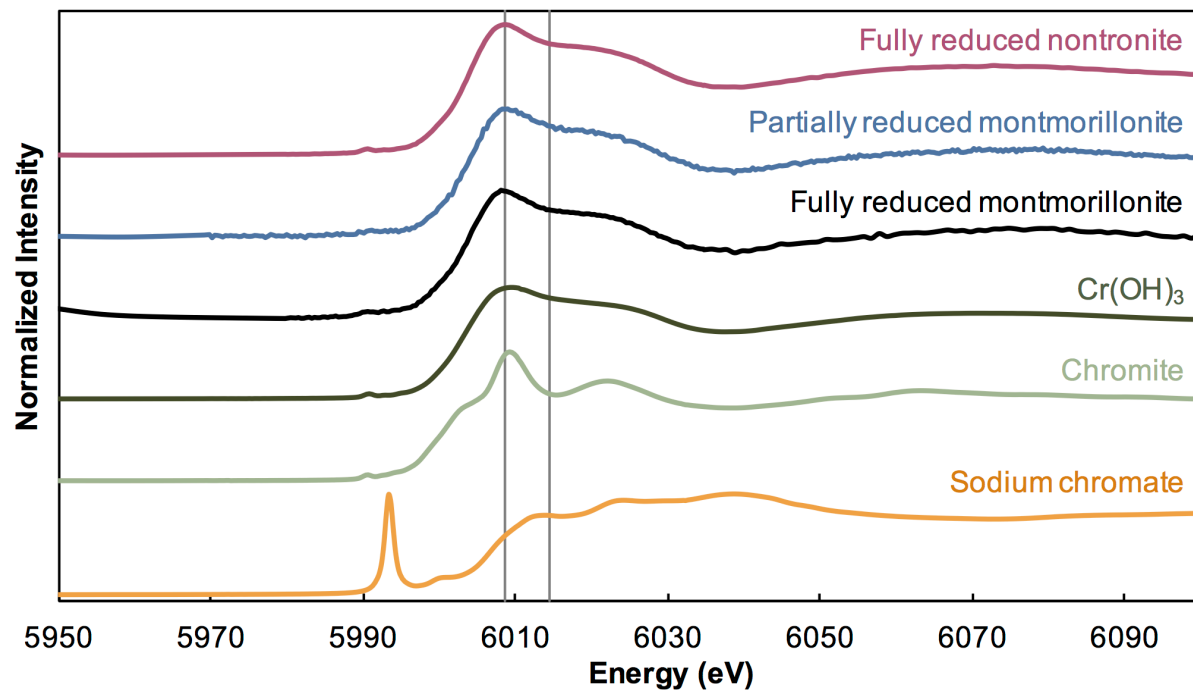


**Figure 6.** Fe XANES spectra of (A) montmorillonite and (B) nontronite in their native, oxidized state (bottom); abiotically reduced with dithionite (middle); and reacted with Cr(VI) after abiotic reduction (top). Cr(aq):Fe(clay mineral) was 0.033 for the montmorillonite and 0.0067 for the nontronite. Both reactors were buffered at pH 7.3. Dotted black lines show least squares linear combination fitting of the reacted clays by the reduced and oxidized spectra.

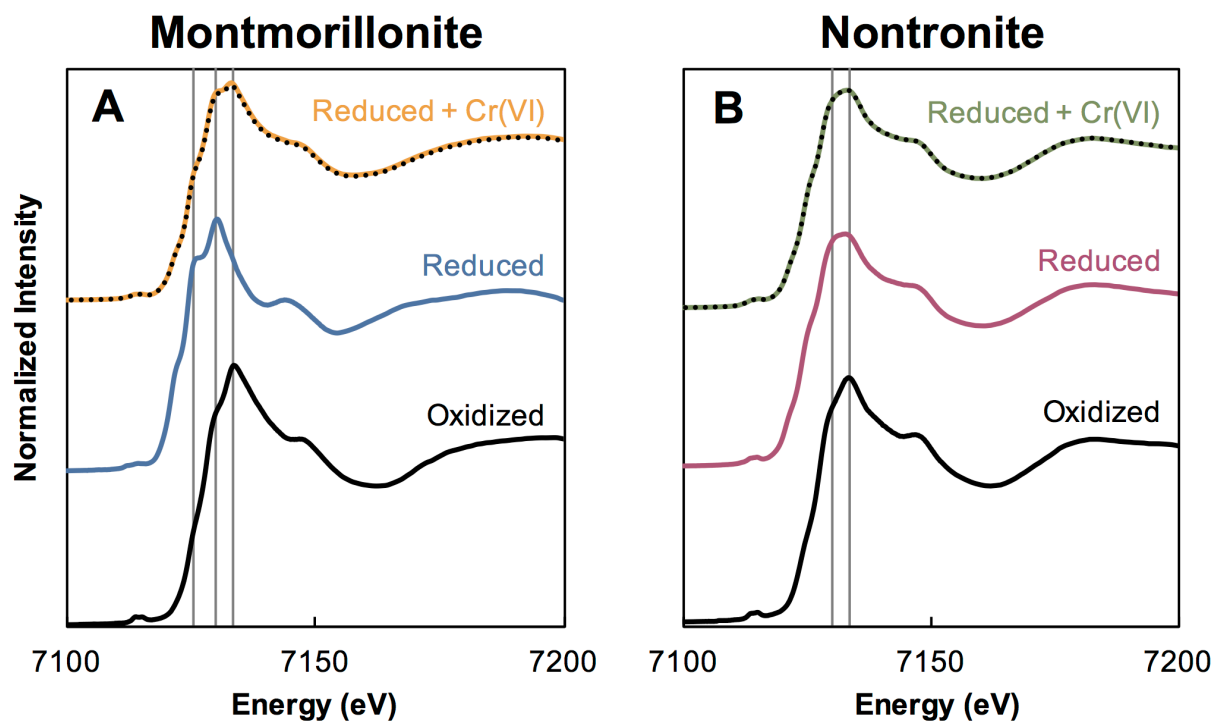
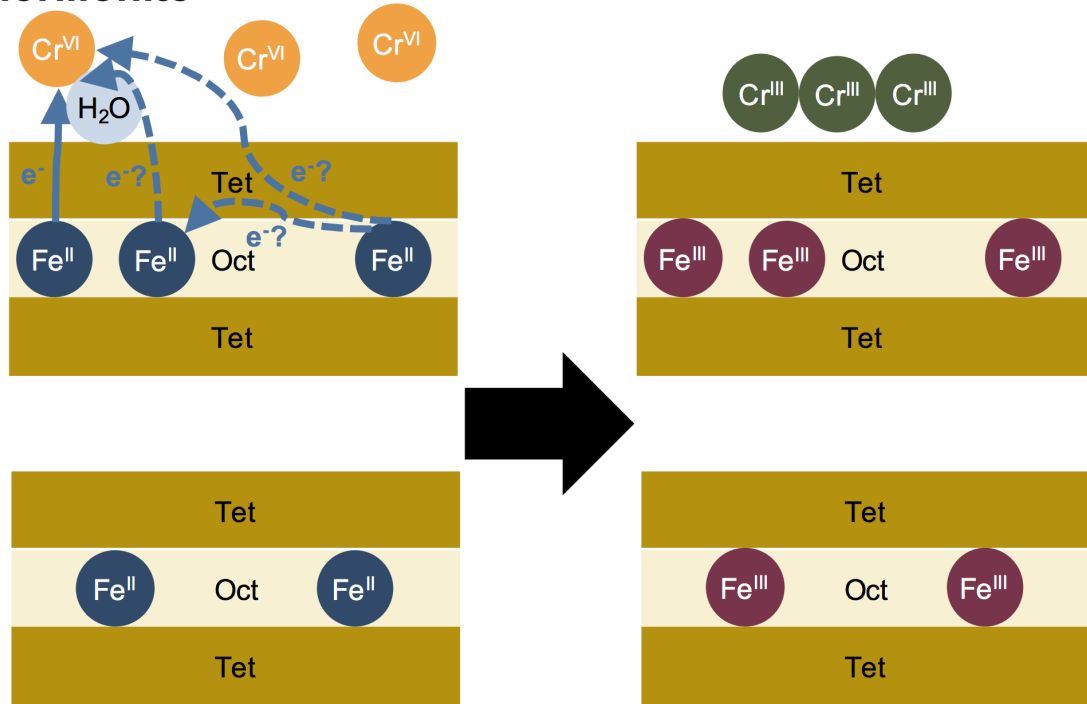


**Figure 7.** Schematic of proposed reaction pathway for montmorillonite (top) and nontronite (bottom). Tet = tetrahedral sheet and Oct = octahedral sheet.

### Montmorillonite



### Nontronite

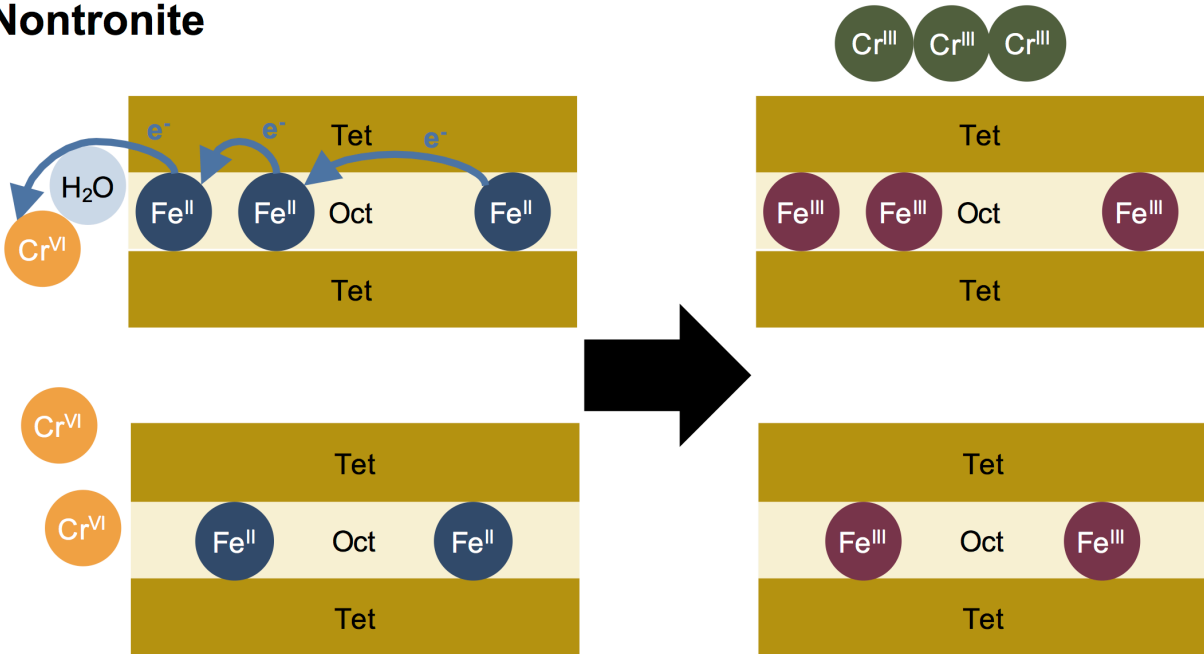
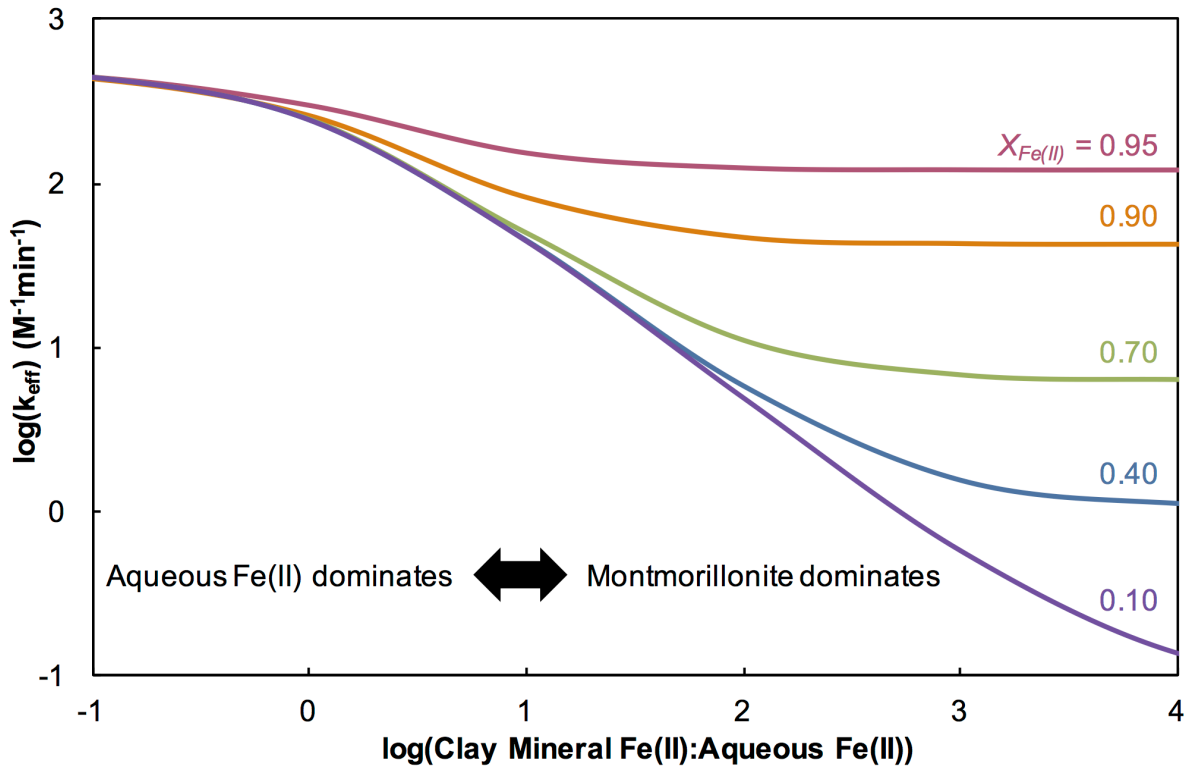


**Figure 8.** Dependence of the effective Cr(VI) reduction rate constant for a montmorillonite-Fe(II) system on the ratio of clay mineral Fe(II): aqueous Fe(II) and  $X_{Fe(II)}$  at pH 5.5. The rate constants for the montmorillonite were derived from the linear fit in Figure 4. The rate constant for aqueous Fe(II) was calculated from Pettine *et al.* (1998).<sup>12</sup>



## ASSOCIATED CONTENT

The following file is available free of charge.

Details about control reactors, kinetic modeling, and XANES and STXM methods; tabulated rate constants; additional Cr and Fe K-edge XANES spectra; STXM images (pdf)

## AUTHOR INFORMATION

### **Corresponding Author**

\* Address: 450 Serra Mall, Bldg. 320, Rm. 118, Stanford, CA 94305, USA

Email address: joewongc@stanford.edu

### **Author Contributions**

The manuscript was written through contributions of all authors. All authors have given approval to the final version of the manuscript.

## ACKNOWLEDGMENTS

This work was supported by National Science Foundation Career Award EAR-1254156 to KM. CJ-W was supported by the United States Department of Defense through a National Defense Science & Engineering Graduate Fellowship and Stanford Graduate Fellowship. XANES spectroscopy was conducted at the Stanford Synchrotron Radiation Lightsource, SLAC National Accelerator Laboratory, a Department of Energy (DOE) Office of Science User Facility. XANES reference spectra were kindly provided by Cynthia McClain and Debra Hausladen. STXM was conducted at the Advanced Light Source, a DOE Office of Science User Facility, and Canadian Light Source.

## REFERENCES

- (1) Oze, C.; Bird, D. K.; Fendorf, S. Genesis of hexavalent chromium from natural sources in soil and groundwater. *Proc. Natl. Acad. Sci.* **2007**, *104* (16), 6544–6549.
- (2) McClain, C. N.; Fendorf, S.; Webb, S. M.; Maher, K. Quantifying Cr(VI) Production and Export from Serpentine Soil of the California Coast Range. *Environ. Sci. Technol.* **2017**, *51* (1), 141–149.
- (3) Dayan, A. D.; Paine, A. J. Mechanisms of chromium toxicity, carcinogenicity and allergenicity: review of the literature from 1985 to 2000. *Hum. Exp. Toxicol.* **2001**, *20* (9), 439–451.
- (4) Anderson, R. A. Chromium as an Essential Nutrient for Humans. *Regul. Toxicol. Pharmacol.* **1997**, *26* (1), S35–S41.
- (5) Rai, D.; Moore, D. A.; Hess, N. J.; Rosso, K. M.; Rao, L.; Heald, S. M. Chromium(III) Hydroxide Solubility in the Aqueous  $K^+$ -H-OH-CO<sub>2</sub>-HCO<sub>3</sub><sup>-</sup>-CO<sub>3</sub><sup>2-</sup>-H<sub>2</sub>O System: A Thermodynamic Model. *J. Solut. Chem.* **2007**, *36* (10), 1261–1285.
- (6) Chebeir, M.; Chen, G.; Liu, H. Emerging investigators series: frontier review: occurrence and speciation of chromium in drinking water distribution systems. *Environ. Sci. Water Res. Technol.* **2016**, *2* (6), 906–914.
- (7) Bartlett, R.; James, B. Behavior of chromium in soils: III. Oxidation. *J. Environ. Qual.* **1979**, *8* (1), 31–35.
- (8) Fendorf, S. E.; Zasoski, R. J. Chromium (III) oxidation by δ-manganese oxide (MnO<sub>2</sub>). 1. Characterization. *Environ. Sci. Technol.* **1992**, *26* (1), 79–85.
- (9) Buerge, I. J.; Hug, S. J. Influence of Organic Ligands on Chromium(VI) Reduction by Iron(II). *Environ. Sci. Technol.* **1998**, *32* (14), 2092–2099.
- (10) Buerge, I. J.; Hug, S. J. Kinetics and pH Dependence of Chromium(VI) Reduction by Iron(II). *Environ. Sci. Technol.* **1997**, *31* (5), 1426–1432.
- (11) Fendorf, S. E.; Li, G. Kinetics of Chromate Reduction by Ferrous Iron. *Environ. Sci. Technol.* **1996**, *30* (5), 1614–1617.
- (12) Pettine, M.; D’Ottone, L.; Campanella, L.; Millero, F. J.; Passino, R. The reduction of chromium (VI) by iron (II) in aqueous solutions. *Geochim. Cosmochim. Acta* **1998**, *62* (9), 1509–1519.
- (13) Doyle, C. S.; Kendelewicz, T.; Brown Jr., G. E. Inhibition of the reduction of Cr(VI) at the magnetite–water interface by calcium carbonate coatings. *Appl. Surf. Sci.* **2004**, *230* (1–4), 260–271.
- (14) Peterson, M. L.; Brown Jr., G. E.; Parks, G. A. Direct XAFS evidence for heterogeneous redox reaction at the aqueous chromium/magnetite interface. *Colloids Surf. Physicochem. Eng. Asp.* **1996**, *107*, 77–88.
- (15) Peterson, M. L.; White, A. F.; Brown Jr., G. E.; Parks, G. A. Surface passivation of magnetite by reaction with aqueous Cr (VI): XAFS and TEM results. *Environ. Sci. Technol.* **1997**, *31* (5), 1573–1576.
- (16) Bishop, M. E.; Glasser, P.; Dong, H.; Arey, B.; Kovarik, L. Reduction and immobilization of hexavalent chromium by microbially reduced Fe-bearing clay minerals. *Geochim. Cosmochim. Acta* **2014**, *133*, 186–203.
- (17) Brigatti, M. F.; Franchini, G.; Lugli, C.; Medici, L.; Poppi, L.; Turci, E. Interaction between aqueous chromium solutions and layer silicates. *Appl. Geochem.* **2000**, *15* (9), 1307–1316.

- (18) Ilton, E. S.; Moses, C. O.; Veblen, D. R. Using X-ray photoelectron spectroscopy to discriminate among different sorption sites of micas: with implications for heterogeneous reduction of chromate at the mica-water interface. *Geochim. Cosmochim. Acta* **2000**, *64* (8), 1437–1450.
- (19) Taylor, R. W.; Shen, S.; Bleam, W. F.; Tu, S.-I. Chromate Removal by Dithionite-Reduced Clays: Evidence from Direct X-ray Adsorption Near Edge Spectroscopy (XANES) of Chromate Reduction at Clay Surfaces. *Clays Clay Miner.* **2000**, *48* (6), 648–654.
- (20) Gan, H.; Bailey, G. W.; Shane Yu, Y. Morphology of lead (II) and chromium (III) reaction products on phyllosilicate surfaces as determined by atomic force microscopy. *Clays Clay Miner.* **1996**, *44* (6), 734–743.
- (21) Brookshaw, D. R.; Coker, V. S.; Lloyd, J. R.; Vaughan, D. J.; Patrick, R. A. D. Redox Interactions Between Cr(VI) and Fe(II) in Bioreduced Biotite and Chlorite. *Environ. Sci. Technol.* **2014**, *48* (19), 11337–11342.
- (22) Butler, E. C.; Chen, L.; Hansel, C. M.; Krumholz, L. R.; Elwood Madden, A. S.; Lan, Y. Biological versus mineralogical chromium reduction: potential for reoxidation by manganese oxide. *Env. Sci Process. Impacts* **2015**, *17* (11), 1930–1940.
- (23) Luan, F.; Gorski, C. A.; Burgos, W. D. Linear Free Energy Relationships for the Biotic and Abiotic Reduction of Nitroaromatic Compounds. *Environ. Sci. Technol.* **2015**, *49* (6), 3557–3565.
- (24) Cervini-Silva, J. Linear free-energy relationship analysis of the fate of chlorinated 1- and 2-carbon compounds by redox-manipulated smectite clay minerals. *Environ. Toxicol. Chem.* **2003**, *22* (10), 2298–2305.
- (25) Jaisi, D. P.; Dong, H.; Plymale, A. E.; Fredrickson, J. K.; Zachara, J. M.; Heald, S.; Liu, C. Reduction and long-term immobilization of technetium by Fe(II) associated with clay mineral nontronite. *Chem. Geol.* **2009**, *264* (1–4), 127–138.
- (26) Bishop, M. E.; Dong, H.; Kukkadapu, R. K.; Liu, C.; Edelman, R. E. Bioreduction of Fe-bearing clay minerals and their reactivity toward pertechnetate (Tc-99). *Geochim. Cosmochim. Acta* **2011**, *75* (18), 5229–5246.
- (27) Ilton, E. S.; Veblen, D. R. Chromium sorption by phlogopite and biotite in acidic solutions at 25°C: Insights from X-ray photoelectron spectroscopy and electron microscopy. *Geochim. Cosmochim. Acta* **1994**, *58* (13), 2777–2788.
- (28) Ilton, E. S.; Veblen, D. R.; Moses, C. O.; Raeburn, S. P. The catalytic effect of sodium and lithium ions on coupled sorption-reduction of chromate at the biotite edge-fluid interface. *Geochim. Cosmochim. Acta* **1997**, *61* (17), 3543–3563.
- (29) Fendorf, S. E.; Lamble, G. M.; Stapleton, M. G.; Kelley, M. J.; Sparks, D. L. Mechanisms of chromium(III) sorption on silica. 1. Chromium(III) surface structure derived by extended x-ray absorption fine structure spectroscopy. *Environ. Sci. Technol.* **1994**, *28* (2), 284–289.
- (30) Fitts, J. P.; Brown Jr., G. E.; Parks, G. A. Structural Evolution of Cr(III) Polymeric Species at the  $\gamma$ -Al<sub>2</sub>O<sub>3</sub>/Water Interface. *Environ. Sci. Technol.* **2000**, *34* (24), 5122–5128.
- (31) Buerge, I. J.; Hug, S. J. Influence of Mineral Surfaces on Chromium(VI) Reduction by Iron(II). *Environ. Sci. Technol.* **1999**, *33* (23), 4285–4291.
- (32) Alexandrov, V.; Neumann, A.; Scherer, M. M.; Rosso, K. M. Electron Exchange and Conduction in Nontronite from First-Principles. *J. Phys. Chem. C* **2013**, *117* (5), 2032–2040.

- (33) Merola, R. B.; McGuire, M. M. Crystallographic Site Distribution and Redox Activity of Fe in Nontronites Determined by Optical Spectroscopy. *Clays Clay Miner.* **2009**, *57* (6), 771–778.
- (34) Alexandrov, V.; Rosso, K. M. Insights into the Mechanism of Fe(II) Adsorption and Oxidation at Fe–Clay Mineral Surfaces from First-Principles Calculations. *J. Phys. Chem. C* **2013**, *117* (44), 22880–22886.
- (35) Neumann, A.; Olson, T. L.; Scherer, M. M. Spectroscopic Evidence for Fe(II)–Fe(III) Electron Transfer at Clay Mineral Edge and Basal Sites. *Environ. Sci. Technol.* **2013**, *47* (13), 6969–6977.
- (36) Gorski, C. A.; Aeschbacher, M.; Soltermann, D.; Voegelin, A.; Baeyens, B.; Marques Fernandes, M.; Hofstetter, T. B.; Sander, M. Redox Properties of Structural Fe in Clay Minerals. 1. Electrochemical Quantification of Electron-Donating and -Accepting Capacities of Smectites. *Environ. Sci. Technol.* **2012**, *46* (17), 9360–9368.
- (37) Gorski, C. A.; Klüpfel, L.; Voegelin, A.; Sander, M.; Hofstetter, T. B. Redox Properties of Structural Fe in Clay Minerals. 2. Electrochemical and Spectroscopic Characterization of Electron Transfer Irreversibility in Ferruginous Smectite, SWa-1. *Environ. Sci. Technol.* **2012**, *46* (17), 9369–9377.
- (38) Gorski, C. A.; Klüpfel, L. E.; Voegelin, A.; Sander, M.; Hofstetter, T. B. Redox Properties of Structural Fe in Clay Minerals: 3. Relationships between Smectite Redox and Structural Properties. *Environ. Sci. Technol.* **2013**, *47* (23), 13477–13485.
- (39) Ridley, M. *Summary Conclusions for the Pilot in-Situ Chromium Reduction Test at Riverbank Army Ammunitions Plant*; UCRL-TR-231326; Lawrence Livermore National Laboratory (LLNL): Livermore, CA, 2007.
- (40) Ludwig, R. D.; Su, C.; Lee, T. R.; Wilkin, R. T.; Acree, S. D.; Ross, R. R.; Keeley, A. In Situ Chemical Reduction of Cr(VI) in Groundwater Using a Combination of Ferrous Sulfate and Sodium Dithionite: A Field Investigation. *Environ. Sci. Technol.* **2007**, *41* (15), 5299–5305.
- (41) Fruchter, J. S.; Cole, C. R.; Williams, M. D.; Vermeul, V. R.; Amonette, J. E.; Szecsody, J. E.; Istok, J. D.; Humphrey, M. D. Creation of a Subsurface Permeable Treatment Zone for Aqueous Chromate Contamination Using In Situ Redox Manipulation. *Ground Water Monit. Remediat.* **2000**, *20* (2), 66–77.
- (42) Vantelon, D.; Montarges-Pelletier, E.; Michot, L. J.; Pelletier, M.; Thomas, F.; Briois, V. Iron distribution in the octahedral sheet of dioctahedral smectites. An Fe K-edge X-ray absorption spectroscopy study. *Phys. Chem. Miner.* **2003**, *30* (1), 44–53.
- (43) Schaefer, M. V.; Gorski, C. A.; Scherer, M. M. Spectroscopic Evidence for Interfacial Fe(II)–Fe(III) Electron Transfer in a Clay Mineral. *Environ. Sci. Technol.* **2011**, *45* (2), 540–545.
- (44) Mermut, A. R.; Cano, A. F. Baseline Studies of the Clay Minerals Society Source Clays: Chemical Analyses of Major Elements. *Clays Clay Miner.* **2001**, *49* (5), 381–386.
- (45) Gates, W. P.; Slade, P. G.; Manceau, A.; Lanson, B. Site Occupancies by Iron in Nontronites. *Clays Clay Miner.* **2002**, *50* (2), 223–239.
- (46) Chipera, S. J.; Bish, D. L. Baseline Studies of the Clay Minerals Society Source Clays: Powder X-Ray Diffraction Analyses. *Clays Clay Miner.* **2001**, *49* (5), 398–409.
- (47) Keeling, J. L.; Raven, M. D.; Gates, W. P. Geology and characterization of two hydrothermal nontronites from weathered metamorphic rocks at the Uley graphite mine, South Australia. *Clays Clay Miner.* **2000**, *48* (5), 537–548.

- (48) Soltermann, D.; Baeyens, B.; Bradbury, M. H.; Fernandes, M. M. Fe(II) Uptake on Natural Montmorillonites. II. Surface Complexation Modeling. *Environ. Sci. Technol.* **2014**, *48* (15), 8698–8705.
- (49) Stucki, J. W.; Golden, D. C.; Roth, C. B. Preparation and handling of dithionite-reduced smectite suspensions. *Clays Clay Min.* **1984**, *32* (3), 191–197.
- (50) Stucki, J. W. A review of the effects of iron redox cycles on smectite properties. *Comptes Rendus Geosci.* **2011**, *343* (2–3), 199–209.
- (51) Ribeiro, F. R.; Fabris, J. D.; Kostka, J. E.; Komadel, P.; Stucki, J. W. Comparisons of structural iron reduction in smectites by bacteria and dithionite: II. A variable-temperature Mössbauer spectroscopic study of Garfield nontronite. *Pure Appl. Chem.* **2009**, *81* (8), 1499–1509.
- (52) Komadel, P.; Lear, P. R.; Stucki, J. W. Reduction and reoxidation of nontronite: Extent of reduction and reaction rates. *Clays Clay Miner.* **1990**, *38* (2), 203–208.
- (53) Stucki, J. W.; Su, K.; Pentráková, L.; Pentrák, M. Methods for handling redox-sensitive smectite dispersions. *Clay Miner.* **2014**, *49* (3), 359–377.
- (54) Russell, J. D.; Goodman, B. A.; Fraser, A. R. Infrared and Mössbauer studies of reduced nontronites. *Clays Clay Miner.* **1979**, *27* (1), 63–71.
- (55) Drits, V. A.; Manceau, A. A Model for the Mechanism of Fe<sup>3+</sup> to Fe<sup>2+</sup> Reduction in Dioctahedral Smectites. *Clays Clay Miner.* **2000**, *48* (2), 185–195.
- (56) Tombácz, E.; Szekeres, M. Colloidal behavior of aqueous montmorillonite suspensions: the specific role of pH in the presence of indifferent electrolytes. *Appl. Clay Sci.* **2004**, *27* (1–2), 75–94.
- (57) Jaisi, D. P.; Liu, C.; Dong, H.; Blake, R. E.; Fein, J. B. Fe<sup>2+</sup> sorption onto nontronite (NAu-2). *Geochim. Cosmochim. Acta* **2008**, *72* (22), 5361–5371.
- (58) Environmental Protection Agency. *EPA Method 7196A; Test Methods for Evaluating Solid Waste, Physical/Chemical Methods; 7196A; Environmental Protection Agent.*
- (59) Stookey, L. L. Ferrozine—a new spectrophotometric reagent for iron. *Anal. Chem.* **1970**, *42* (7), 779–781.
- (60) Webb, S. M. SIXpack: a graphical user interface for XAS analysis using IFEFFIT. *Phys. Scr.* **2005**, *2005* (T115), 1011.
- (61) Ravel, B.; Newville, M. Athena, Artemis, Hephaestus: data analysis for X-ray absorption spectroscopy using IFEFFIT. *J. Synchrotron Radiat.* **2005**, *12* (4), 537–541.
- (62) O’Day, P. A.; Rivera, N.; Root, R.; Carroll, S. A. X-ray absorption spectroscopic study of Fe reference compounds for the analysis of natural sediments. *Am. Mineral.* **2004**, *89* (4), 572–585.
- (63) Neumann, A.; Hofstetter, T. B.; Lüssi, M.; Cirpka, O. A.; Petit, S.; Schwarzenbach, R. P. Assessing the Redox Reactivity of Structural Iron in Smectites Using Nitroaromatic Compounds As Kinetic Probes. *Environ. Sci. Technol.* **2008**, *42* (22), 8381–8387.
- (64) Neumann, A.; Hofstetter, T. B.; Skarpeli-Liati, M.; Schwarzenbach, R. P. Reduction of Polychlorinated Ethanes and Carbon Tetrachloride by Structural Fe(II) in Smectites. *Environ. Sci. Technol.* **2009**, *43* (11), 4082–4089.
- (65) Marcus, R. A.; Sutin, N. Electron transfers in chemistry and biology. *Biochim. Biophys. Acta BBA - Rev. Bioenerg.* **1985**, *811* (3), 265–322.
- (66) Pauling, L. The Principles Determining the Structure of Complex Ionic Crystals. *J. Am. Chem. Soc.* **1929**, *51* (4), 1010–1026.

- (67) Sposito, G. *The Chemistry of Soils*, 2 edition.; Oxford University Press: Oxford; New York, 2008.
- (68) Ball, J. W.; Nordstrom, D. K. Critical Evaluation and Selection of Standard State Thermodynamic Properties for Chromium Metal and Its Aqueous Ions, Hydrolysis Species, Oxides, and Hydroxides. *J. Chem. Eng. Data* **1998**, *43* (6), 895–918.
- (69) Brown Jr., G. E.; Parks, G. A. Sorption of Trace Elements on Mineral Surfaces: Modern Perspectives from Spectroscopic Studies, and Comments on Sorption in the Marine Environment. *Int. Geol. Rev.* **2001**, *43* (11), 963–1073.
- (70) Zachara, J. M.; Cowan, C. E.; Schmidt, R. L.; Ainsworth, C. C. Chromate adsorption by kaolinite. *Clays Clay Min.* **1988**, *36* (4), 317–326.
- (71) Wu, C.-H.; Lo, S.-L.; Lin, C.-F. Competitive adsorption of molybdate, chromate, sulfate, selenate, and selenite on  $\gamma$ -Al<sub>2</sub>O<sub>3</sub>. *Colloids Surf. Physicochem. Eng. Asp.* **2000**, *166* (1), 251–259.
- (72) Sander, M.; Hofstetter, T. B.; Gorski, C. A. Electrochemical Analyses of Redox-Active Iron Minerals: A Review of Nonmediated and Mediated Approaches. *Environ. Sci. Technol.* **2015**, *49* (10), 5862–5878.
- (73) Marcus, R. A. Chemical and electrochemical electron-transfer theory. *Annu. Rev. Phys. Chem.* **1964**, *15* (1), 155–196.
- (74) Marcus, R. A. On the Theory of Electron-Transfer Reactions. VI. Unified Treatment for Homogeneous and Electrode Reactions. *J. Chem. Phys.* **1965**, *43* (2), 679–701.
- (75) Gorski, C. A.; Nurmi, J. T.; Tratnyek, P. G.; Hofstetter, T. B.; Scherer, M. M. Redox Behavior of Magnetite: Implications for Contaminant Reduction. *Environ. Sci. Technol.* **2010**, *44* (1), 55–60.
- (76) Klausen, J.; Troeber, S. P.; Haderlein, S. B.; Schwarzenbach, R. P. Reduction of substituted nitrobenzenes by Fe (II) in aqueous mineral suspensions. *Environ. Sci. Technol.* **1995**, *29* (9), 2396–2404.
- (77) Manceau, A.; Drits, V. A.; Lanson, B.; Chateigner, D.; Wu, J.; Huo, D.; Gates, W. P.; Stucki, J. W. Oxidation-reduction mechanism of iron in dioctahedral smectites: II. Crystal chemistry of reduced Garfield nontronite. *Am. Mineral.* **2000**, *85* (1), 153–172.
- (78) Jaisi, D. P.; Dong, H.; Morton, J. P. Partitioning of Fe(II) in Reduced Nontronite (NAu-2) to Reactive Sites: Reactivity in Terms of Tc(VII) Reduction. *Clays Clay Miner.* **2008**, *56* (2), 175–189.
- (79) Wu, T.; Griffin, A. M.; Gorski, C. A.; Shelobolina, E. S.; Xu, H.; Kukkadapu, R. K.; Roden, E. E. Interactions Between Fe(III)-oxides and Fe(III)-phyllosilicates During Microbial Reduction 2: Natural Subsurface Sediments. *Geomicrobiol. J.* **2017**, *34* (3), 231–241.

# Supporting Information

**Kinetics and Products of Chromium(VI) Reduction  
by Iron(II/III)-Bearing Clay Minerals**  
*Claresta Joe-Wong<sup>1</sup>, Gordon E. Brown, Jr.<sup>1,2</sup>, Kate Maher<sup>1</sup>*

<sup>1</sup>Department of Geological Sciences, School of Earth, Energy & Environmental Sciences,  
Stanford University, Stanford, CA 94305, USA

<sup>2</sup>Department of Photon Science and Stanford Synchrotron Radiation Lightsource, SLAC  
National Accelerator Laboratory, 2575 Sand Hill Road, MS 69, Menlo Park, CA 94025, USA

Total Number of Pages: 18  
Total Number of Tables: 3  
Total Number of Figures: 10

## List of Contents

Control Reactors

Kinetic Modeling

X-Ray Absorption Near Edge Structure Spectroscopy

Scanning Transmission X-Ray Microscopy

References

## List of Tables

**Table S1.** Second-order rate constants for Cr(VI) reduction by nontronite.

**Table S2.** Second-order rate constants for Cr(VI) reduction by montmorillonite.

**Table S3.** Reaction stoichiometry.

## List of Figures

**Figure S1.** Fe XANES spectra of reduced clay minerals.

**Figure S2.** Aqueous Cr(VI) concentrations in control reactors containing oxidized clay minerals.

**Figure S3.** Aqueous Cr(VI) concentrations and pseudo-first-order kinetics.

**Figure S4.** Comparison of pseudo-first-order kinetics.

**Figure S5.** Cr XANES spectra showing the effects of pH on the Cr products.

**Figure S6.** Cr XANES spectra showing the effects of Cr(aq):Fe(clay mineral) ratio on the Cr products.

**Figure S7.** Fe XANES spectra for the fully reduced nontronite after 2 weeks of reaction with stoichiometric Cr(VI).

**Figure S8.** Second order rate constants of Cr(VI) reduction as a function of average  $X_{Fe(III)}$ .

**Figure S9.** STXM images of abiotically reduced nontronite reacted with Cr(VI).

**Figure S10.** STXM image of the abiotically reduced nontronite.

## Control Reactors

Control reactors containing 10  $\mu\text{M}$  Cr(VI) and 0.5 mM HEPES or acetate showed no decrease in Cr(VI) concentrations over the course of a week. Similarly, reactors containing 10-100  $\mu\text{M}$  Cr(VI) and oxidized clays did not show significant decreases in Cr(VI) concentrations over the course of a week (**Figure S2**).

## Kinetic Modeling

A second-order rate law was assumed in order to compare clays with different values of  $X_{Fe(II)}$ . A derivation of the linearized rate law is presented below:

$$\frac{d[\text{Cr(VI)}]}{dt} = -k[\text{Cr(VI)}] \left( \frac{X_{Fe(II)} \times f_{Fe} \times d_{clay}}{MW_{Fe}} \right) \quad (1)$$

where the last term will be denoted as  $[\text{Fe(II)}]$  for convenience. The rate law corresponds to the nominal elementary reaction  $\text{Cr(VI)} + \text{Fe(II)} \rightarrow \text{intermediates} + \text{products}$  and can be solved using the dummy variable  $x$  for the progress of the elementary reaction:

$$\frac{dx}{dt} = k([\text{Cr(VI)}]_0 - x)([\text{Fe(II)}]_0 - x) \quad (2)$$

$$\frac{dx}{([\text{Cr(VI)}]_0 - x)([\text{Fe(II)}]_0 - x)} = k dt \quad (3)$$

$$\int_0^x \frac{dx}{([\text{Cr(VI)}]_0 - x)([\text{Fe(II)}]_0 - x)} = \int_0^t k dt \quad (4)$$

The left side can be integrated using the method of partial fractions:

$$\frac{1}{[\text{Cr(VI)}]_0 - [\text{Fe(II)}]_0} \left( \ln \left( \frac{[\text{Fe(II)}]_0}{([\text{Fe(II)}]_0 - x)} \right) - \ln \left( \frac{[\text{Cr(VI)}]_0}{([\text{Cr(VI)}]_0 - x)} \right) \right) = kt \quad (5)$$

$$\frac{1}{[\text{Cr(VI)}]_0 - [\text{Fe(II)}]_0} \left( \ln \left( \frac{[\text{Fe(II)}]_0([\text{Cr(VI)}]_0 - x)}{[\text{Cr(VI)}]_0([\text{Fe(II)}]_0 - x)} \right) \right) = kt \quad (6)$$

$$\ln \left( \frac{([\text{Cr(VI)}]_0 - x)}{([\text{Fe(II)}]_0 - x)} \right) = kt([\text{Cr(VI)}]_0 - [\text{Fe(II)}]_0) - \ln \left( \frac{[\text{Fe(II)}]_0}{[\text{Cr(VI)}]_0} \right) \quad (7)$$

$$\ln \left( \frac{[\text{Cr(VI)}]}{[\text{Fe(II)}]} \right) = kt([\text{Cr(VI)}]_0 - [\text{Fe(II)}]_0) + \ln \left( \frac{[\text{Cr(VI)}]_0}{[\text{Fe(II)}]_0} \right) \quad (8)$$

This shows a linear relationship between  $\ln([\text{Cr(VI)}]/[\text{Fe(II)}])$  and  $t$  with slope  $m$  such that

$$k = \frac{m}{[\text{Cr(VI)}]_0 - [\text{Fe(II)}]_0} \quad (9)$$

The relationship between  $E_{eff}^\circ$  and  $X_{Fe(II)}$  is governed by a modified Nernst equation:<sup>1</sup>

$$E_h = E_h^\circ - \frac{1}{\beta} 0.059 \log \left( \frac{X_{Fe(II)}}{1 - X_{Fe(II)}} \right) \quad (10)$$

$$E_h = E_{eff}^\circ - 0.059 \log \left( \frac{X_{Fe(II)}}{1 - X_{Fe(II)}} \right) \quad (11)$$

where  $E_h^\circ$  and  $\beta$  are constants tabulated in Gorski *et al.* (2013).<sup>2</sup> Combining these equations,

$$E_{eff}^\circ = E_h^\circ - \left( \frac{\beta - 1}{\beta} \right) 0.059 \log \left( \frac{X_{Fe(II)}}{1 - X_{Fe(II)}} \right) \quad (12)$$

Linear free energy relationships between  $E_{eff}^\circ$  and  $\log(k)$  were determined through linear least-squares fitting. Using eq 12 to convert between  $E_{eff}^\circ$  and  $X_{Fe(II)}$ , the corresponding relationships between  $X_{Fe(II)}$  and  $\log(k)$  are shown in **Figure S8**.

### **X-Ray Absorption Near Edge Structure Spectroscopy**

Chromium and Fe XANES spectroscopy was performed at beamlines 4-1 and 11-2 at the Stanford Synchrotron Radiation Lightsource using a Si (220) crystal at  $\phi = 90^\circ$ . After reaction, samples were centrifuged, and the partially dried solids were sandwiched between Cr- and Fe-free Kapton tape and mounted at room temperature in a He-purged sample chamber. The beam was detuned by 50% to minimize harmonics. A Ge array detector was used to measure sample fluorescence, and XANES spectra were collected in 0.2 eV increments around the Cr and Fe absorption edges. Neither a filter nor Soller slits was used for Cr spectra due to the low signal. The K-edge spectrum of Cr metal foil was taken simultaneously with every sample, and the first maximum of the first derivative was calibrated to 5989.0 eV. For Fe, a Mn filter and Soller slits were used to reduce signal noise. The K-edge spectrum of Fe metal foil was taken simultaneously with every sample, and the first maximum of the first derivative was calibrated to 7112.0 eV. No changes in Fe or Cr spectra after repeated scanning were observed, indicating that beam damage was minimal.

### **Scanning Transmission X-Ray Microscopy**

STXM was performed at beamline 5.3.2.2 at the Advanced Light Source and the Soft X-ray Spectromicroscopy beamline at the Canadian Light Source. Iron and Cr maps were collected below the L2 edge for each element (700.0 and 570.0 eV, respectively) and at the L2 maximum-intensity energy for each oxidation state (708.0 and 710.0 eV for Fe(II) and Fe(III), respectively; 578.0 and 580.5 eV for Cr(III) and Cr(VI), respectively).<sup>3,4</sup> Maps were iteratively aligned and converted from transmission to optical density. For both Fe and Cr, the below-edge background map was subtracted from each above-edge map, generating maps of the relative intensities for each oxidation state.

STXM images of the partially reacted nontronite reveal that Cr(III) is evenly distributed on the basal surface of the clay particles (**Figure S9**). The particle edges do not show any buildup of Cr(III), whose migration to the basal plane may be assisted by complexation with the HEPES or acetate buffers. Precipitation on the basal surface or in the interlayer space instead of at the edges is consistent with the lack of passivation of the nontronite particle surfaces, which would be expected if Cr(III) precipitated at the reaction sites.<sup>5,6</sup> The distribution of Fe(II/III) in the reacted nontronite is more ambiguous: Fe(III) appears to be concentrated in areas of greater clay density, but this may be an artifact of image processing. Bulk Fe XANES spectra do not support the formation of Fe(III)-rich phases. In the reduced nontronite not yet reacted with Cr(VI), Fe(II) and Fe(III) are evenly distributed (**Figure S10**).

## References

- (1) Gorski, C. A.; Klüpfel, L.; Voegelin, A.; Sander, M.; Hofstetter, T. B. Redox Properties of Structural Fe in Clay Minerals. 2. Electrochemical and Spectroscopic Characterization of Electron Transfer Irreversibility in Ferruginous Smectite, SWa-1. *Environ. Sci. Technol.* **2012**, *46* (17), 9369–9377.
- (2) Gorski, C. A.; Klüpfel, L. E.; Voegelin, A.; Sander, M.; Hofstetter, T. B. Redox Properties of Structural Fe in Clay Minerals: 3. Relationships between Smectite Redox and Structural Properties. *Environ. Sci. Technol.* **2013**, *47* (23), 13477–13485.
- (3) Bourdelle, F.; Benzerara, K.; Beyssac, O.; Cosmidis, J.; Neuville, D. R.; Brown Jr., G. E.; Paineau, E. Quantification of the ferric/ferrous iron ratio in silicates by scanning transmission X-ray microscopy at the Fe L<sub>2,3</sub> edges. *Contrib. Mineral. Petrol.* **2013**, *166* (2), 423–434.
- (4) Christl, I.; Imseng, M.; Tatti, E.; Frommer, J.; Viti, C.; Giovannetti, L.; Kretzschmar, R. Aerobic Reduction of Chromium(VI) by *Pseudomonas corrugata* 28: Influence of Metabolism and Fate of Reduced Chromium. *Geomicrobiol. J.* **2012**, *29* (2), 173–185.
- (5) Peterson, M. L.; White, A. F.; Brown Jr., G. E.; Parks, G. A. Surface passivation of magnetite by reaction with aqueous Cr (VI): XAFS and TEM results. *Environ. Sci. Technol.* **1997**, *31* (5), 1573–1576.
- (6) Doyle, C. S.; Kendelewicz, T.; Brown Jr., G. E. Inhibition of the reduction of Cr(VI) at the magnetite–water interface by calcium carbonate coatings. *Appl. Surf. Sci.* **2004**, *230* (1–4), 260–271.

**Table S1.** Montmorillonite kinetics.  $X_{Fe(II)}$  is the average over the course of the experiment. All experiments at pH 7.3 were buffered by sodium HEPES; all experiments at pH 5.5 were buffered by sodium acetate.  $\log(k)$  standard deviations are from replicate experiments. The number of replicates is given in parentheses in the third column.  $R^2$  values are for the linear least-squares fit used to derive  $k$ .

pH	$X_{Fe(II)}$	$\log(k)$ ( $M^{-1}min^{-1}$ )	$R^2$
7.3	0.94	$2.4 \pm 0.3$ (2)	0.92
	0.84	$1.190 \pm 0.003$ (2)	0.99
	0.67	$0.8 \pm 0.3$ (3)	0.92
	0.49	$0.114 \pm 0.007$ (2)	0.98
	0.34	$-0.35 \pm 0.05$ (2)	0.98
5.5	0.94	$1.9 \pm 0.1$ (2)	0.96
	0.84	$1.5 \pm 0.2$ (2)	0.95
	0.67	$0.39 \pm 0.09$ (2)	0.99
	0.49	$0.53 \pm 0.01$ (2)	0.97
	0.34	$-0.22 \pm 0.02$ (2)	0.93

**Table S2.** Nontronite kinetics.  $X_{Fe(II)}$  is the average over the course of the experiment. All experiments at pH 7.3 were buffered by sodium HEPES; all experiments at pH 5.5 were buffered by sodium acetate.  $\log(k)$  standard deviations are from replicate experiments. The number of replicates is given in parentheses in the third column.  $R^2$  values are for the linear least-squares fit used to derive  $k$ .

pH	$X_{Fe(II)}$	$\log(k)$ ( $M^{-1}min^{-1}$ )	$R^2$
7.3	0.98	$2.9 \pm 0.2$ (4)	0.97
	0.93	$2.6 \pm 0.3$ (2)	0.94
	0.62	$1.22 \pm 0.03$ (3)	0.98
	0.26	$-0.60 \pm 0.17$ (3)	0.91
5.5	0.98	$3.1 \pm 0.3$ (3)	0.98
	0.93	$3.6 \pm 0.1$ (2)	0.98
	0.62	$1.49 \pm 0.01$ (2)	0.98
	0.26	$0.6 \pm 0.3$ (3)	0.91

**Table S3.** Comparison of Fe(II) oxidized after reaction and Cr(VI) removed from solution. Initial and final  $X_{Fe(II)}$  was determined from Fe K-edge XANES spectroscopy. Produced Cr(III) was calculated assuming a 1:3 reaction with Fe(II). Cr(VI) removed from solution was determined spectrophotometrically.

Clay	Initial $X_{Fe(II)}$	$X_{Fe(II)}$ After Reaction with Cr(VI)	Fe(II) Oxidized ( $\mu\text{mol}$ )	Cr(III) Produced ( $\mu\text{mol}$ )	Cr(VI) Removed from Solution ( $\mu\text{mol}$ )
Montmorillonite	$1.00 \pm 0.05$	$0.41 \pm 0.05$	$5.3 \pm 0.9$	$1.8 \pm 0.3$	$1.6 \pm 0.5$
	$1.00 \pm 0.05$	$0.85 \pm 0.05$	$1.4 \pm 0.5$	$0.46 \pm 0.15$	$0.30 \pm 0.02$
Nontronite	$1.00 \pm 0.05$	$0.97 \pm 0.05$	$0.7 \pm 0.9$	$0.24 \pm 0.2$	$0.86 \pm 0.05$
	$1.00 \pm 0.05$	$0.27 \pm 0.05$	$18 \pm 1$	$5.8 \pm 0.4$	$5.3 \pm 1.6$

**Figure S1.** Fe XANES spectra of (A) montmorillonite and (B) nontronite after abiotic reduction with sodium dithionite. Dotted black lines show linear combination fits.

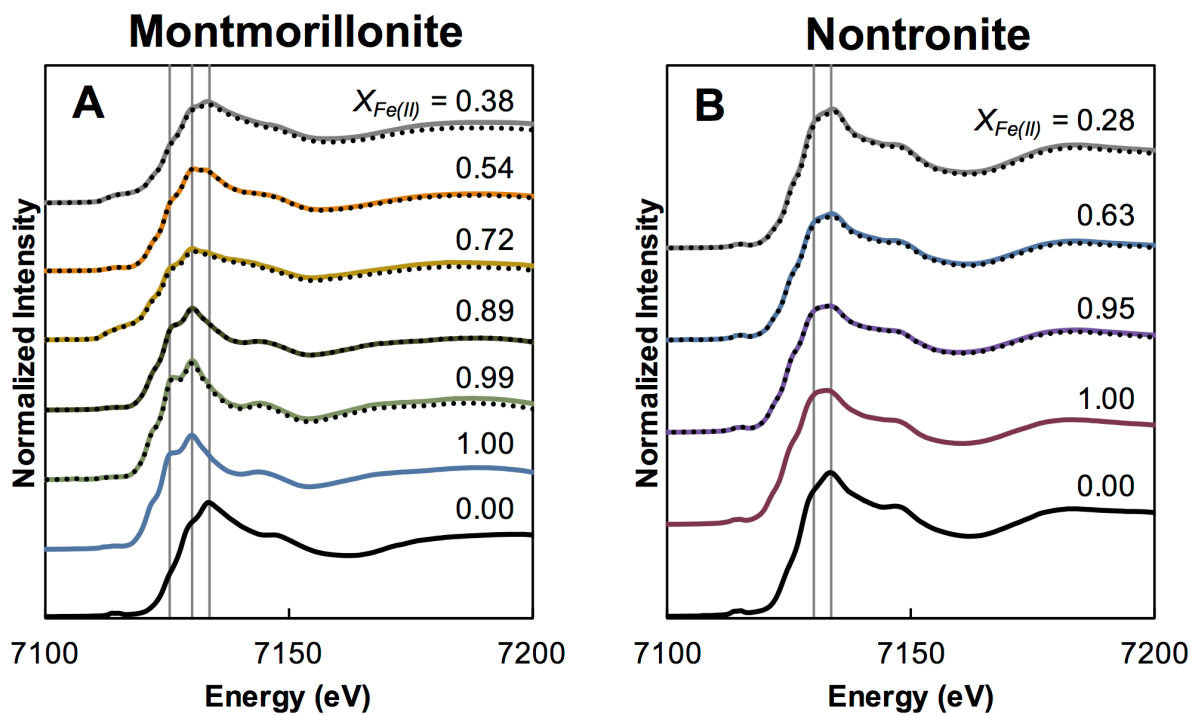


**Figure S2.** Aqueous Cr(VI) concentrations in control reactors containing (A) montmorillonite and (B) nontronite in their natural, fully oxidized state and buffered at pH 7.3. The molar Cr(aq):Fe(clay mineral) ratio was 0.033 for the montmorillonite and 0.017 for the nontronite.  $[\text{Cr(VI)}]_0 = 10 \mu\text{M}$  for both reactors.

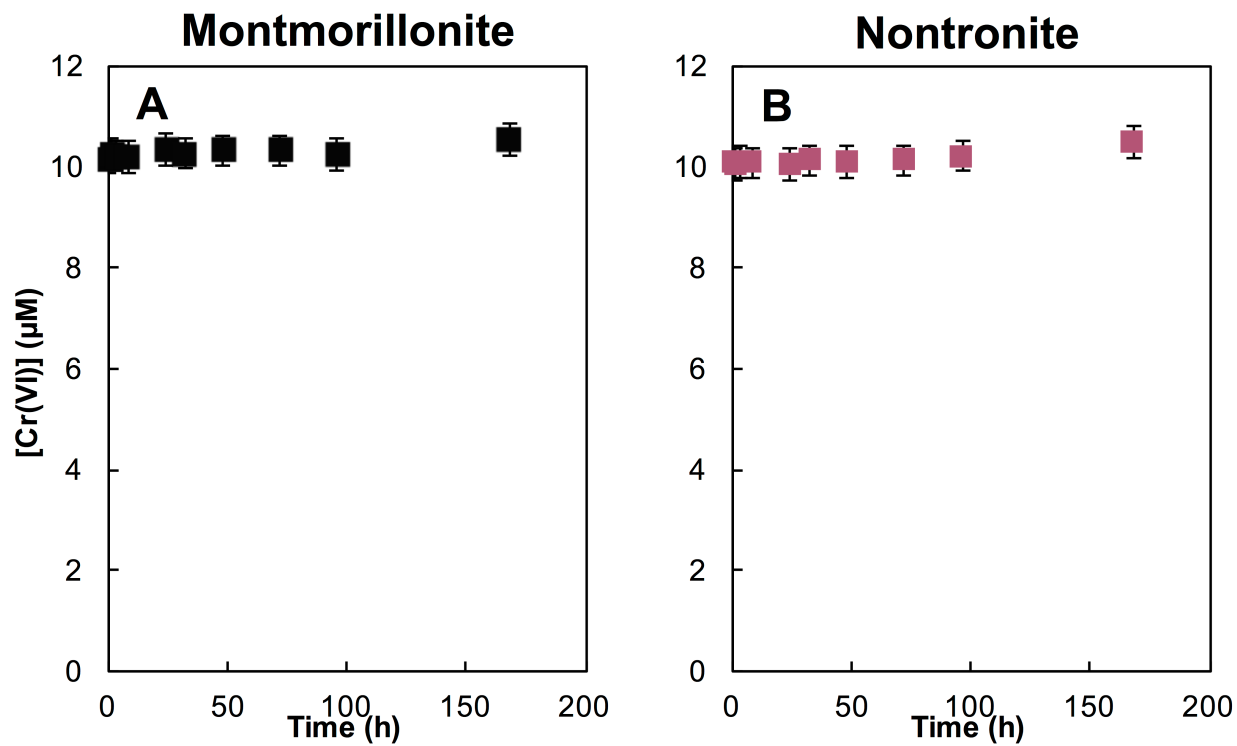


**Figure S3.** (A-B) Aqueous Cr(VI) concentrations and (C-D) pseudo-first-order kinetics in reactors containing (A, C) reduced montmorillonite ( $X_{Fe(II)} = 0.49$ ) and (B, D) reduced nontronite ( $X_{Fe(II)} = 0.98$ ). Both reactors were buffered at pH 7.3, and  $[Cr(VI)]_0 = 10 \mu M$ . Error bars show 3% reproducibility and are in most cases smaller than the symbols.

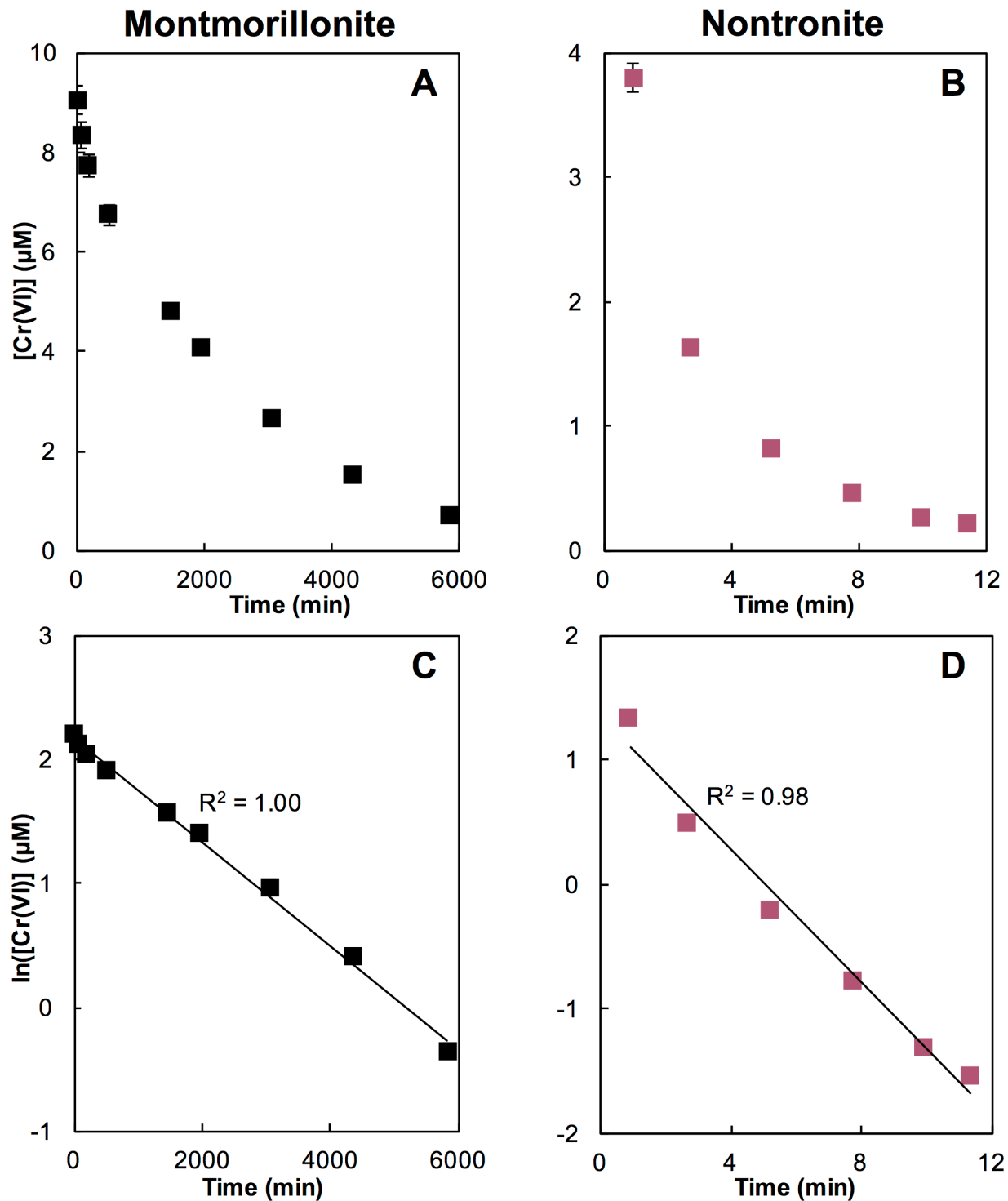


**Figure S4.** Pseudo-first-order kinetics for the reduced nontronite at pH 7.3 ( $X_{Fe(II)} = 0.98$ ). Cr(aq):Fe(clay mineral) is 0.017 for both reactors.  $[Cr(VI)]_0 = 10 \mu M$  for the squares and  $5 \mu M$  for the triangles.

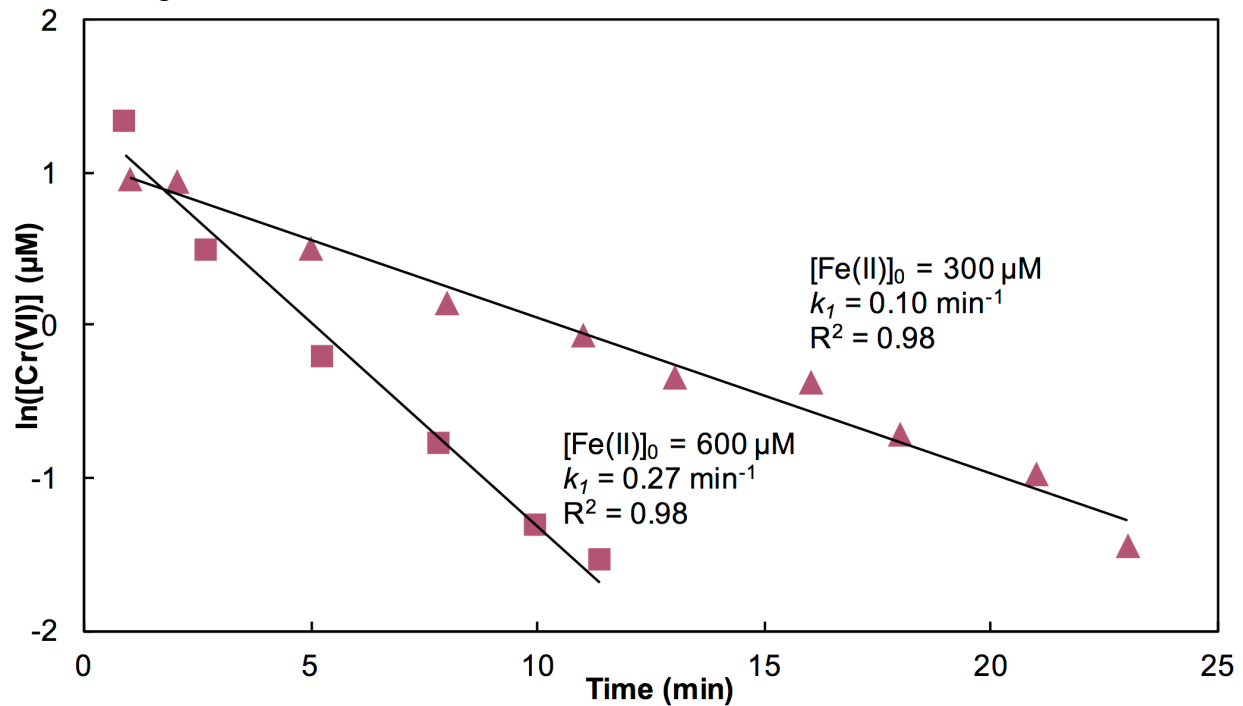


**Figure S5.** Cr XANES spectra showing the effects of pH on the Cr products. Samples at pH 7.3 were buffered by sodium HEPES, and samples at pH 5.5 were buffered by sodium acetate. Cr(aq):Fe(clay mineral) is 0.033 for both montmorillonite spectra and 0.017 for both nontronite spectra. Both clays were fully reduced prior to reaction with Cr(VI).

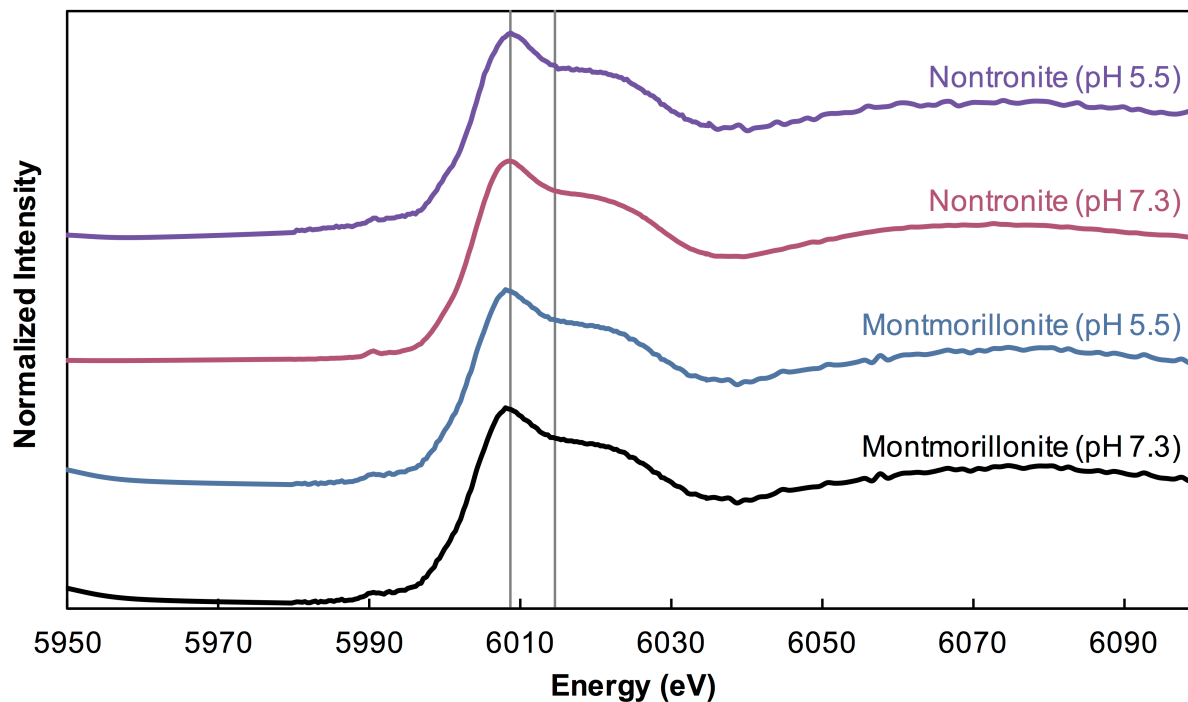


**Figure S6.** Cr XANES spectra showing the effects of Cr(aq):Fe(clay mineral) on the Cr products. All reactors were buffered at pH 7.3.

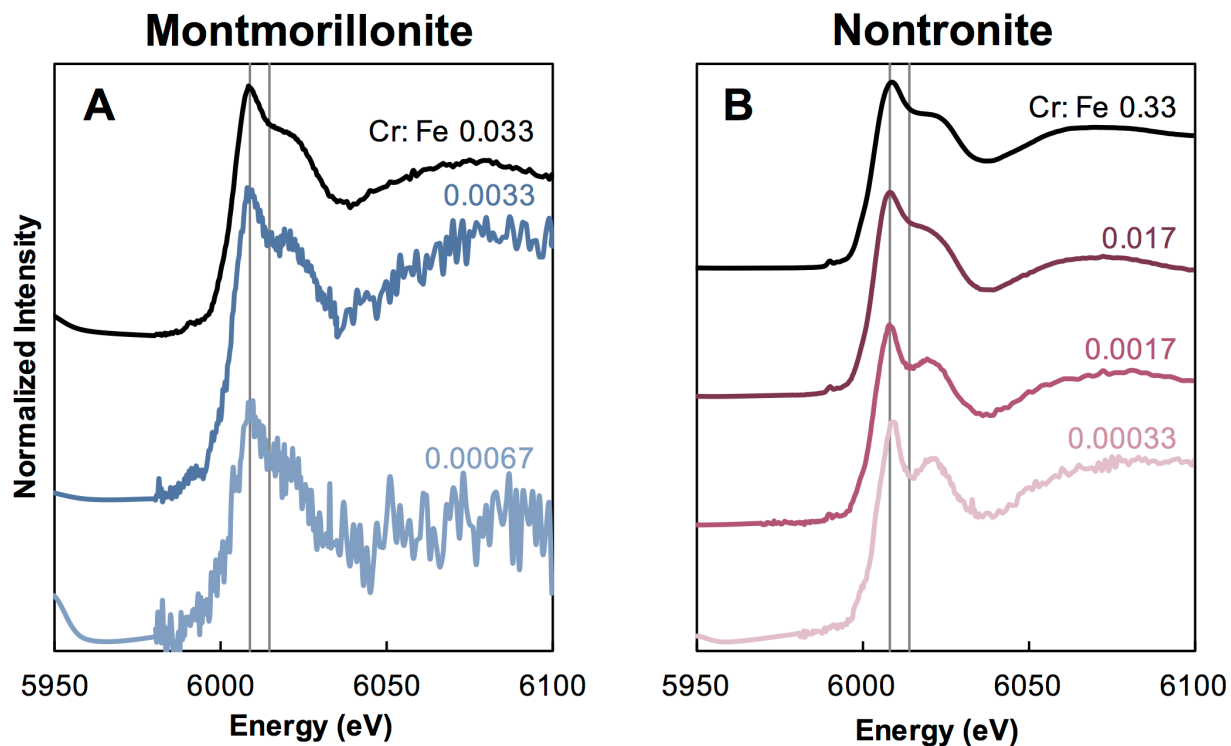


**Figure S7.** Fe XANES spectra for the fully reduced nontronite after 2 weeks of reaction with stoichiometric Cr(VI). The sample at pH 7.3 was buffered by sodium HEPES, and the sample at pH 5.5 was buffered by sodium acetate. Dotted black lines show linear combination fits.

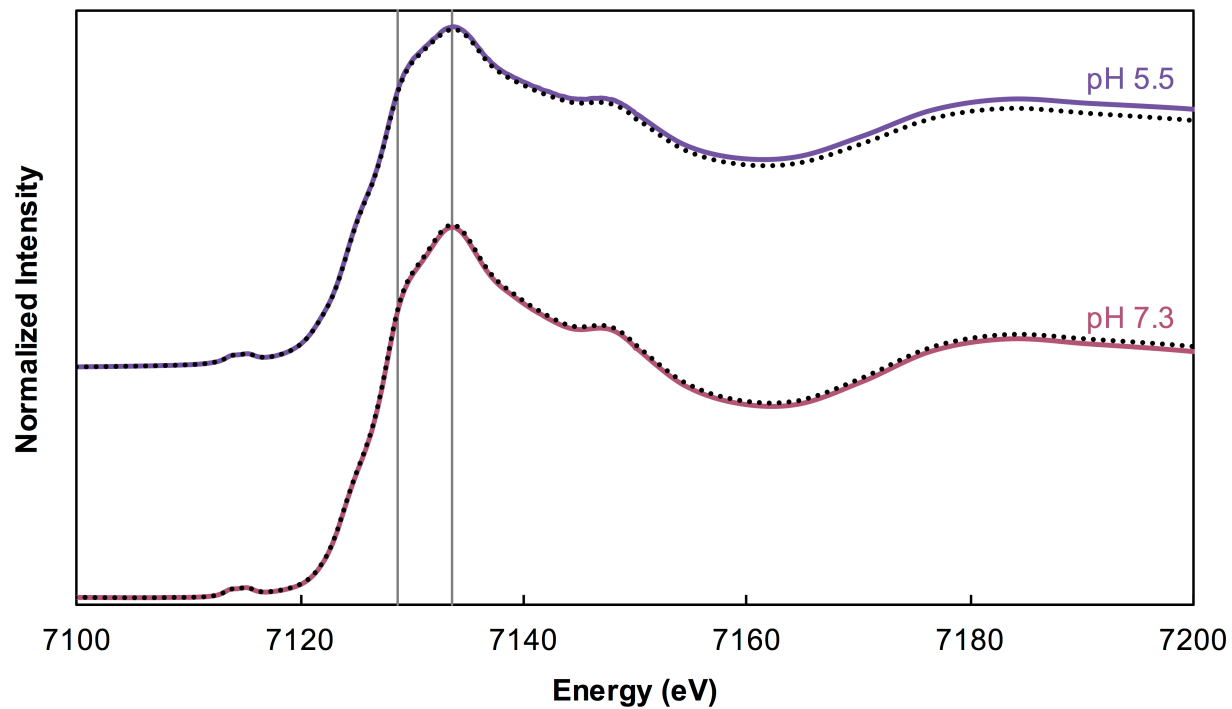


**Figure S8.** Second-order rate constants of Cr(VI) reduction as a function of average  $X_{Fe(II)}$  for (A) montmorillonite and (B) nontronite. Rate constants at pH 7.3 are shown as filled squares; rate constants at pH 5.5 are shown as open circles. Lines represent linear least-squares fit for  $\log(k)$  vs.  $E_{eff}^{\circ}$ . Vertical error bars show standard deviations for replicate experiments. Horizontal error bars show 5% error for linear combination fitting for  $X_{Fe(II)}$ .

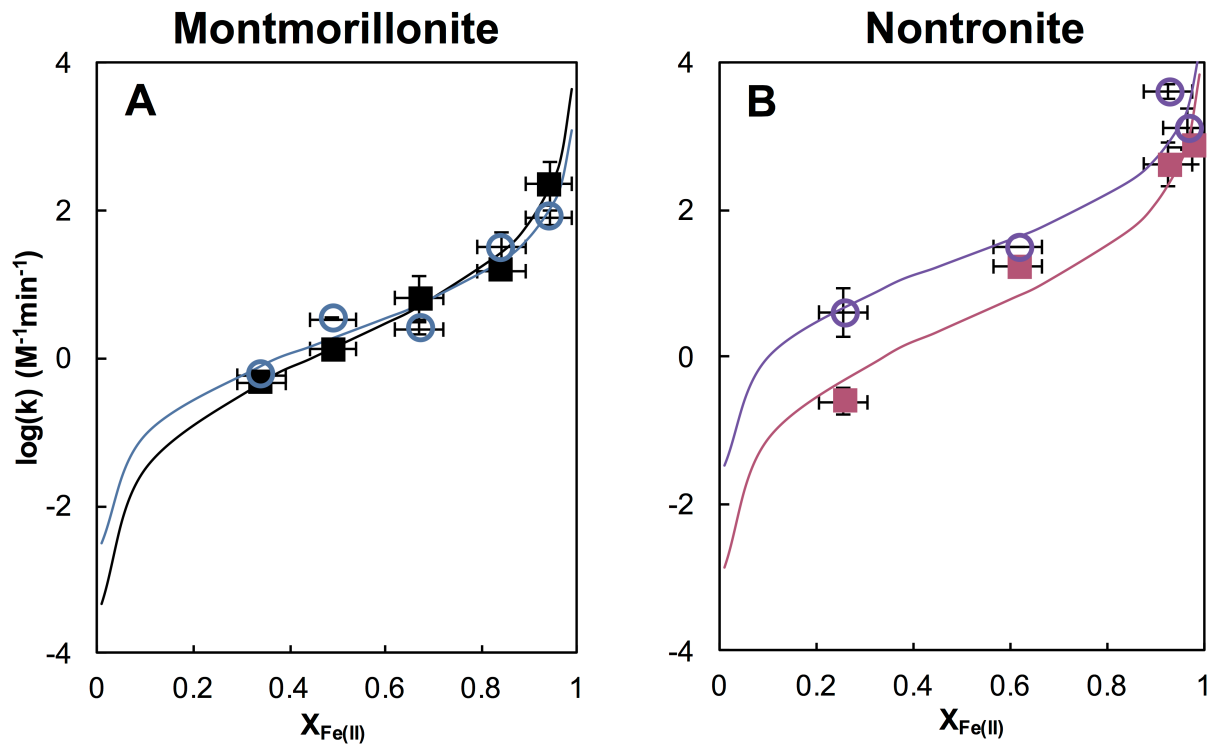


**Figure S9.** STXM images of abiotically reduced nontronite reacted with Cr(VI) at pH 7.3. A shows optical density; B shows distribution of Fe(II) (blue) and Fe(III) (red) for the same area; inset on A shows distribution of Cr(VI) (red) and Cr(III) (blue) for a subset of the area. Blue-red scale is arbitrary.

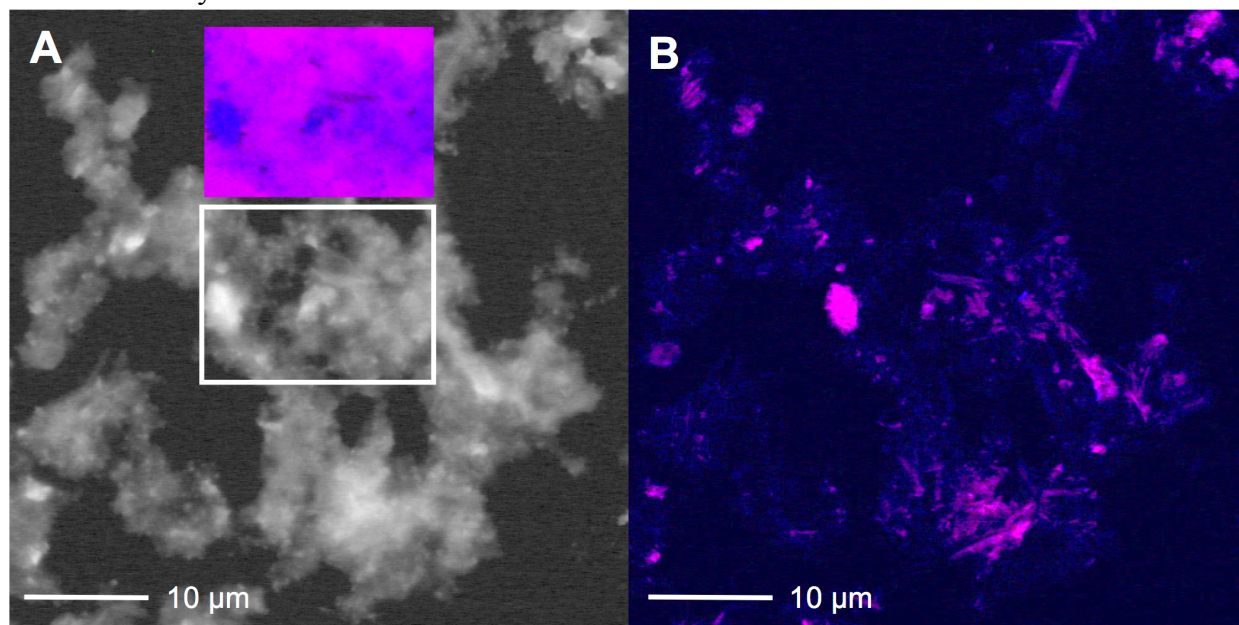


**Figure S10.** STXM image of the abiotically reduced nontronite showing A) optical density and B) distribution of Fe(II) (blue) and Fe(III) (red) for the same area. Blue-red scale is arbitrary.

